Topical Report 1

Turbulent Flame Speeds and NOx Kinetics of HHC Fuels with Contaminants and High Dilution Levels

For the Period:
October 1, 2010 – September 30, 2011

Principal Authors:
Eric Petersen, Michael Krejci, Olivier Mathieu, Andrew Vissotski, Sankar Ravi, Travis Sikes, Anthony Levacque, and Christopher Aul

Principal Investigator:
Eric L. Petersen
Department of Mechanical Engineering
Texas A&M University
3123 TAMU
College Station, TX 77843
407-823-6123

Issue Date: November 28, 2011

DOE Award No. DE-FE0004679
TEES Project 32525-B1730

Prepared for:
U. S. Department of Energy/NETL
626 Cochrans Mill Road
P.O. Box 10940
Pittsburgh, PA 15236-0940

ABSTRACT

This progress report documents the first year of the project, from October 1, 2010 through September 30, 2011. Laminar flame speeds and ignition delay times have been measured for hydrogen and various compositions of H_2/CO (syngas) at elevated pressures and elevated temperatures. Two constant-volume cylindrical vessels were used to visualize the spherical growth of the flame through the use of a schlieren optical setup to measure the laminar flame speed of the mixture. Hydrogen experiments were performed at initial pressures up to 10 atm and initial temperatures up to 443 K. A syngas composition of 50/50 was chosen to demonstrate the effect of carbon monoxide on H_2-O_2 chemical kinetics at standard temperature and pressures up to 10 atm. All atmospheric mixtures were diluted with standard air, while all elevated-pressure experiments were diluted with a He:O_2 of 7:1 to minimize hydrodynamic instabilities. The laminar flame speed measurements of hydrogen and syngas are compared to available literature data over a wide range of equivalence ratios where good agreement can be seen with several data sets. Additionally, an improved chemical kinetics model is shown for all conditions within the current study. The model and the data presented herein agree well, which demonstrates the continual, improved accuracy of the chemical kinetics model.

A high-pressure shock tube was used to measure ignition delay times for several baseline compositions of syngas at three pressures across a wide range of temperatures. The compositions of syngas (H_2/CO) presented in this study include 80/20, 50/50, 40/60, 20/80, and 10/90, all of which are compared to previously published ignition delay times from a hydrogen-oxygen mixture to demonstrate the effect of carbon monoxide addition. Generally, an increase in carbon monoxide increases the ignition delay time, but there does seem to be a pressure dependency. At low temperatures and pressures higher than about 12 atm, the ignition delay times appear to be indistinguishable with an increase in carbon monoxide. However, at high temperatures the composition of H_2 and CO has a strong influence on ignition delay times. Model agreement is good across the range of the study, particularly at the elevated pressures. Also an increase in carbon monoxide causes the activation energy of the mixture to decrease.

TABLE OF CONTENTS

ABSTRACT....1
TABLE OF CONTENTS....2
EXECUTIVE SUMMARY....3
APPROACH....4
RESULTS AND DISCUSSION....5
TASK 1 – PROJECT MANAGEMENT AND PROGRAM PLANNING....5
TASK 2 – TURBULENT FLAME SPEED MEASUREMENTS OF SYNGAS MIXTURES....7
TASK 3 – LAMINAR FLAME SPEED MEASUREMENTS WITH DILUENTS....13
TASK 4 – NOX MECHANISM VALIDATION EXPERIMENTS....24
TASK 5 – FUNDAMENTAL NOX KINETICS....31
TASK 6 – EFFECT OF IMPURITIES ON SYNGAS KINETICS....35
CONCLUSION....41
COST STATUS....42
SCHEDULE/MILESTONE STATUS....43
REFERENCES....44
APPENDIX A – LAMINAR FLAME SPEED DATA....48

EXECUTIVE SUMMARY

This effort is concerned with the chemical kinetics of fuel blends with high-hydrogen content in the presence of high levels of dilutions and impurities. Emphasis is on the use of ignition delay times and flame speeds to elucidate the diluent and impurity effects on the fuel chemistry at gas turbine engine conditions and to also validate the chemical kinetics models. The project is divided into six primary tasks: 1) Project Management and Program Planning; 2) Turbulent Flame Speed Measurements of Syngas Mixtures; 3) Laminar Flame Speed Measurements with Diluents; 4) NOx Mechanism Validation Experiments; 5) Fundamental NOx Kinetics; and 6) Effect of Impurities on Syngas Kinetics. This Topical Report documents the first year of the project, from October 1, 2010 through September 30, 2011.

Two constant-volume cylindrical vessels were used to visualize the spherical growth of the flame through the use of a schlieren optical setup to measure the laminar flame speed of the mixture. Hydrogen experiments were performed at initial pressures up to 10 atm and initial temperatures up to 443 K. A syngas composition of 50/50 was chosen to demonstrate the effect of carbon monoxide on H_2-O_2 chemical kinetics at standard temperature and pressures up to 10 atm. All atmospheric mixtures were diluted with standard air, while all elevated-pressure experiments were diluted with a He:O_2 of 7:1 to minimize hydrodynamic instabilities. The laminar flame speed measurements of hydrogen and syngas are compared to available literature data over a wide range of equivalence ratios where good agreement can be seen with several data sets.

A high-pressure shock tube was used to measure ignition delay times for several baseline compositions of syngas at three pressures across a wide range of temperatures. The compositions of syngas (H_2/CO) presented in this study include 80/20, 50/50, 40/60, 20/80, and 10/90, all of which are compared to previously published ignition delay times from a hydrogen-oxygen mixture to demonstrate the effect of carbon monoxide addition. Model agreement is good across the range of the study, particularly at the elevated pressures. Also an increase in carbon monoxide causes the activation energy of the mixture to decrease.

The $H_2/O_2/NO_2$ system, highly diluted in Argon, was investigated thanks to shock-tube ignition delay time measurements with the purpose to understand the sensitizing effect of NO_2 addition on hydrogen oxidation. Experiments and computational simulations were performed at an equivalence ratio of 0.5, at pressures of approximately 1.5, 13 and 30 atm and at temperatures from 980 – 1750 K. At around 1.5 atm, the ignition delay time is not sensitive to additions of 100 or 400 ppm of NO_2. An addition of 1600 ppm will however increase the ignition delay time. At a pressure of 13.5 atm, the ignition delay time was significantly decreased by addition of 100 and 400 ppm below 1140 K. Above 1140 K, no effect on the ignition delay time was observed for a NO_2 addition of 400 ppm or less. A NO_2 addition of 1600 ppm will decrease the delay time compared to the neat hydrogen conditions below 1140 K. The delays are however longer than the delays obtained with 400 ppm of NO_2. Above 1140 K, the delay time is increased by this large addition of NO_2. At 30 atm, the delay time is decreased by NO_2 addition, the decrease being more important as the temperature is lowered. The delays obtained with 1600 ppm of NO_2 are slightly longer than the delays obtained with 400 ppm of NO_2. A sensitivity analysis was performed at 13.5 atm to help explain the interesting effects of the addition of various amounts of NO_2 on the ignition delay time. These experimental results were explained in terms of detailed kinetic reactions and chemical process using the sensitivity analysis.

APPROACH

The basic approach is best summarized by the six main tasks, as follows.

Task 1 – Project Management and Program Planning
Project management includes the submission of regular and required reports to DOE, in addition to routine management of the TAMU project by the PI. This task also includes the specific interaction with the industry consultants. Feedback from GE, Siemens, Rolls-Royce, and Alstom will be obtained at the beginning of the program through face-to-face meetings, followed by periodic contact throughout the project.

Task 2 – Turbulent Flame Speed Measurements of Syngas Mixtures
The original flame speed vessel at Texas A&M University will be modified with the capability to perform turbulent flame speed measurements. Turbulence will be generated with fans, and the experiment and turbulence level will be well characterized prior to performing experiments. Turbulent flame speeds will be measured as a function of turbulence level, mixture composition, and initial pressure. Correlations will be developed that relate the turbulent speed to the equivalent laminar flame speed for the same mixture and initial pressure.

Task 3 –Laminar Flame Speed Measurements with Diluents
Using the new, heated flame speed vessel, high-pressure experiments up to 20 atm will be conducted over a wide range of syngas mixtures. These mixtures will have realistic levels of diluents, with emphasis on high levels of water dilution. The heated facility will allow for such mixtures, with initial temperatures as high as 600 K possible. The resulting database will be compared with current chemical kinetics models and will be used as the baseline for the turbulent flame speed measurements.

Task 4 – NOx Mechanism Validation Experiments
These experiments will involve shock tubes to obtain data for validation of the NOx submechanism at realistic ranges of mixture composition, stoichiometry, and pressure. Emphasis will be placed on two types of experiments: 1) ignition experiments (both dilute and high concentration) containing initial levels of NO_2 and N_2O, to test the mechanisms in a global way, and 2) dilute experiments wherein key intermediate and NOx-related species profiles are measured using laser absorption and ir emission techniques. The resulting database will be compared to the NOx mechanism, and areas for improvement will be identified as needed.

Task 5 – Fundamental NOx Kinetics
Focus for this task will be on the direct measurement of specific rate coefficients to improve the accuracy of the NOx predictions at conditions involving high hydrogen and dilution levels. We anticipate the focus to be on the NNH pathway, and the rate measurement will be done in carefully designed shock tube experiments at controlled conditions.

Task 6 – Effect of Impurities on Syngas Kinetics
This task will involve primarily ignition measurements from the shock-tube experiments that contain realistic levels of syngas impurities. Consultation with industry will be helpful in identifying the likely impurities. Flame speed measurements can also be performed to assess the impact of the most important or likely impurities.

RESULTS AND DISCUSSION

Progress during this reporting period is presented within the context of the six primary tasks.

TASK 1 – PROJECT MANAGEMENT AND PROGRAM PLANNING

Efforts during the first quarter focused on getting the project set up, outlining the tasks for the students workers and with partners at The Aerospace Corporation, and overseeing the preparation of the experimental facilities for their use on the present project. Students were identified for the project, including one Ph.D. student, Sankar Ravi, devoted entirely to Task 2 (turbulent flame speeds) and one M.S. student, Michael Krejci, on the laminar flame speed experiments (Tasks 2 and 3). These two students along with a third (Ph.D.) student, Andrew Vissotski (on separate funding) comprise the core of the flame speed group within the PI's laboratory. A postdoctoral researcher, Dr. Olivier Mathieu, was identified for working on the shock-tube experiments (primarily Task 6, plus Task 4). He began in late March, 2011, and was covered partly under the matching funding for the portion of his time devoted to this program. Shock-tube students include (part time each) Christopher Aul (Task 5) and John Pemelton (Task 4). A visiting graduate student researcher from Orleans, France helped out with the shock-tube experiments for four months in the summer of 2011, covered mostly under discretionary funding and funding from France.

One important aspect of the project (see timeline) is the interaction with the industry advisory panel, primarily to obtain feedback and information on the relevant syngas mixtures and operating conditions of interest to the gas turbine community. While some efforts in this area were made during this first quarter, notably with our Rolls-Royce Canada contacts, we decided to finalize the target mixtures and related information from the industry team in the second quarter. This decision was made because a visit to the General Electric Energy facility in South Carolina is scheduled for late January, 2011. Discussions between the PI and GE engineers with regard to the present project will take place during that visit.

As a part of Task 5 and also Task 6, the shock-tube facility at The Aerospace Corporation provides a key component to the present project. Namely, the facility at Aerospace is capable of elevated-pressure and heated experiments for syngas mixtures containing high water content [Petersen et al., 2005]. Most importantly to the present project, the tunable laser absorption diagnostic to be used in the detailed kinetic measurements in Task 5 is located in the Aerospace facility in Los Angeles, CA. In preparation for the use of the facility and laser diagnostic (as part of the long, ongoing relationship between the PI's research group and the Aerospace team of Dr. Mark Crofton and Dr. Andrea Hsu), the PI visited the Aerospace Corporation facility to begin setting up for the project experiments. Christopher Aul also visited the laboratory at Aerospace Corporation and will be spending the entire summer of 2011 in Los Angeles to begin the Task 5 tests.

Most of the efforts under the management task during the second quarter were routine. Significant was the interaction with the project's Industrial Advisory Panel. Rather than a single meeting, it proved more convenient to interact with the industry participants individually. A meeting was held with GE Energy in Greenville, SC on January 24-26, 2011. The PI met with Joel Hall and other engineers in the combustion group there, with emphasis on their syngas

work. GE suggested a list of possible contaminants that might cause concern, including H_2S, NH_3, NOx compounds, and carbonyls. Other suggested impurities include lower-order hydrocarbons and water. All of these species were in line with what the PI anticipated. Typical mixtures were also suggested. Communication with Dr. Gilles Bourque of Rolls-Royce and Dr. Felix Güthe of Alstom also took place during this quarter. Feedback from Rolls-Royce and Alstom with regard to possible syngas mixtures and combustion issues was similar to that provided by GE.

During the week of June 19 in the third quarter of this project, the PI was invited to a meeting in India at the Indian Institute of Science in Bangalore. This was a workshop on biofuel combustion, and the PI presented materials and results from the present project, among other material. Matching funds expected from Rolls-Royce Canada for the first year of the project were delayed and were not made available in this first project year; there will be available in the 5^{th} quarter of the project.

TASK 2 – TURBULENT FLAME SPEED MEASUREMENTS OF SYNGAS MIXTURES

An extensive literature search was conducted during the first project year. Presented in Appendix A of the second quarterly report is a bibliography of the 30 references most relevant to the present study.

Measurement of flame speed by optically tracking the growth of a spherically expanding flame in intense, nearly isotropic turbulence with negligible mean flow is a subject of several studies [Bradley et al., 2003; Kido et al., 1996]. Turbulence was induced in all these studies by the use of mixing fans whose rotational speeds can be precisely controlled to induce increasing level of turbulence intensities. The facilities described in these studies are spherical, thus enabling symmetric placement of fans to create a central region of turbulence. The flame speed vessel in Texas A&M University is cylindrical (12" ID x 12" L), and hence a trial and error approach will be adopted to decide on the number and locations of the fans so as to extend the region of turbulence to the entire region of optical access (12.7 cm).

A Plexiglas (clear acrylic, actually) model of the flame speed vessel (scaling1:1) was fabricated to study the fluid mechanics phenomena so that the placement and other details related to the fans and the turbulence characteristics can be optimized before modifying the actual flame speed vessel. Plastic DC axial fans (from Sofasco Fans) will be placed at various locations, and particle image velocimetry will be used to characterize the turbulence generated. The model provides optical access for laser measurements. It also provides a convenient way to change the locations of the fans without having to drill into the metal of the actual vessel. Figure 1 provides a schematic of the model vessel, and Fig. 2 shows a photograph of the model rig.

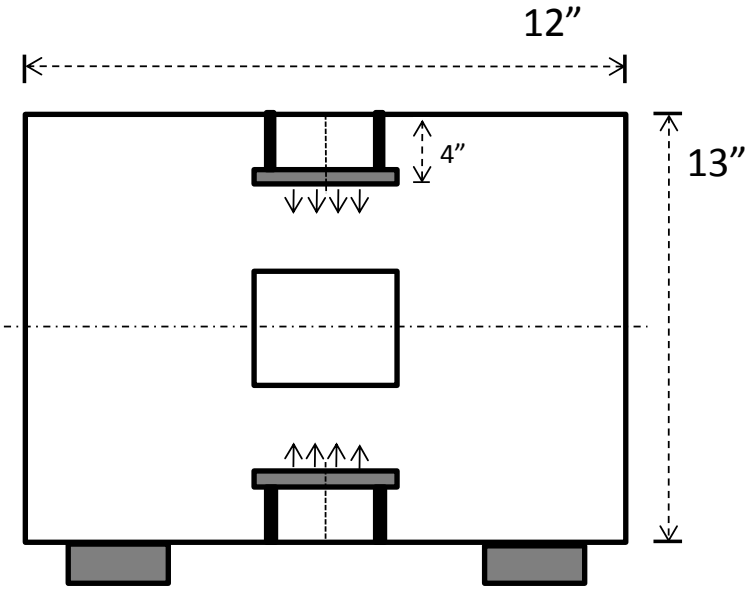

Fig. 1 Schematic diagram of the mock-up rig for testing the placement and performance of the turbulence-generating scheme. The optimized design will be incorporated into the main vessel.

Fig. 2 Photograph of plexiglass mock-up facility showing a trial fan placement.

The study will be conducted in two phases. Phase one focuses on identifying the number of fans needed and their locations in the vessel. The dependence of turbulence characteristics (such as the integral length scales) on the type and size of fans will also be assessed by employing three fan blade types namely, 6 cm and 8 cm backward-curved and 8-cm radial-curved blades.

Once the locations of the fans are finalized, the plastic fans will be replaced with the metal impellers that will be used in the actual flame speed vessel. These metal fans will be connected to motors with speed control and the turbulence statistics [Hwang and Eaton, 2004] will be estimated for a range of rpm. This is the second phase of the study.

Impeller Design- Taguchi Matrix

As widely reviewed by several studies (Lipatnikov and Chomiak (2002) and references there in), turbulent flame speed exhibits a strong dependence on both the thermo-chemical properties of the mixture as well as the turbulence characteristics of the flow field. The turbulence intensity (u') and the integral length scale are the two most commonly used quantities to characterize turbulence.

The aim of this study is to generate high intensity turbulence (u'>5 m/s) and vary the integral length scales independently. Previous studies [Kwon (1991); Haq (1998)] have reported that the

turbulence intensity varied with the rotational speed of the impeller, while the integral length scale remained constant over a wide range of RPM. Haq (1998) and Kwon (1991) have indicated that the blade design controls the way the eddies are shed from the blade tip, thereby impacting the integral length scale. These are qualitative observations, and further investigation is required to assess the contribution of the impeller blade design on the integral length scale.

In the Plexiglas model of the flame speed vessel, we intend to study the effect of impeller design on the turbulence characteristics. Parameters varied include the fan OD, number of blades in each impeller and the blade angle. Other factors such as fan placement, number of fans and fan width were kept constant as significant variations in them were not possible.

A design of experiments approach (Taguchi L4 Matrix) is considered appropriate. The Taguchi matrix (Table 1) is a statistical tool used to assess contribution of various factors by performing minimum number of experiments. The L-4 matrix is a two level matrix in which each factor (maximum of 3) is assigned a high and a low value. The test matrix dictates the design of the prototypes. The Taguchi matrix reduces the number of tests required by 50% as opposed to a full factorial testing (2^3=8 tests).

Table 1 Taguchi L4 matrix.

	Factors		
Test	**1**	**2**	**3**
1	1	1	1
2	2	1	1
3	1	2	1
4	1	1	2

Table 2 shows the variation for each factor.

Table 2 Parameters varied for fan design of experiments matrix.

Parameters		**Low(1)**	**Hi(2)**
1	Fan OD (Inches)	3	5
2	No of Blades	3	6
3	Blade Pitch (degrees)	20	60

Parameters Assumed Constant

1. Fan Placement – Centered arrangement
2. No of Fans = 4
3. Fan Axial Length = 1.5 inches

Four different prototypes were fabricated by laser sintering using Nylon GF. Four fans of each prototype were manufactured. The prototypes are listed in Table 3. Figure 3 shows the Solid works model of each prototype.

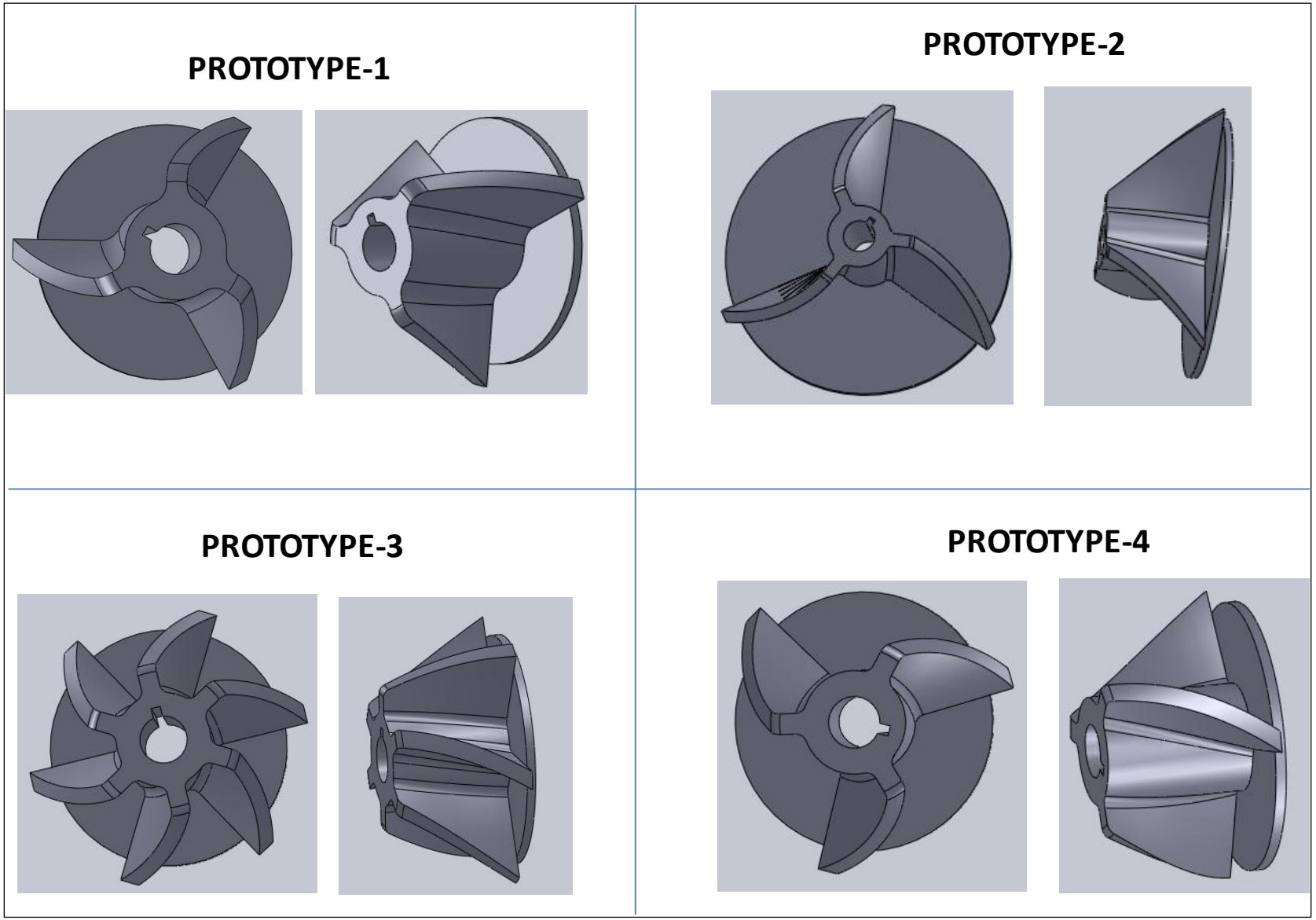

Fig. 3 Impeller prototype designs corresponding to the four configurations in Table 3.

Table 3 Prototypes derived from L4 matrix in Table 1.

Prototype	Fan OD	No of Blades	Blade Pitch
1	3	3	20
2	5	3	20
3	3	6	20
4	3	3	60

Test Matrix

Figures 4 and 5 show the setup of fans within the Plexiglas vessel. Each fan is fitted with a 2.25-hp high-speed motor. The speed of the motors can be varied between 8,000 and 24,000 rpm. Particle Image Velocimetry (PIV) will be used to characterize the flow field inside. Each prototype is to be tested at three speeds namely, 8000, 12000 and 14000 rpm. Thus there will be a total of 12 tests.

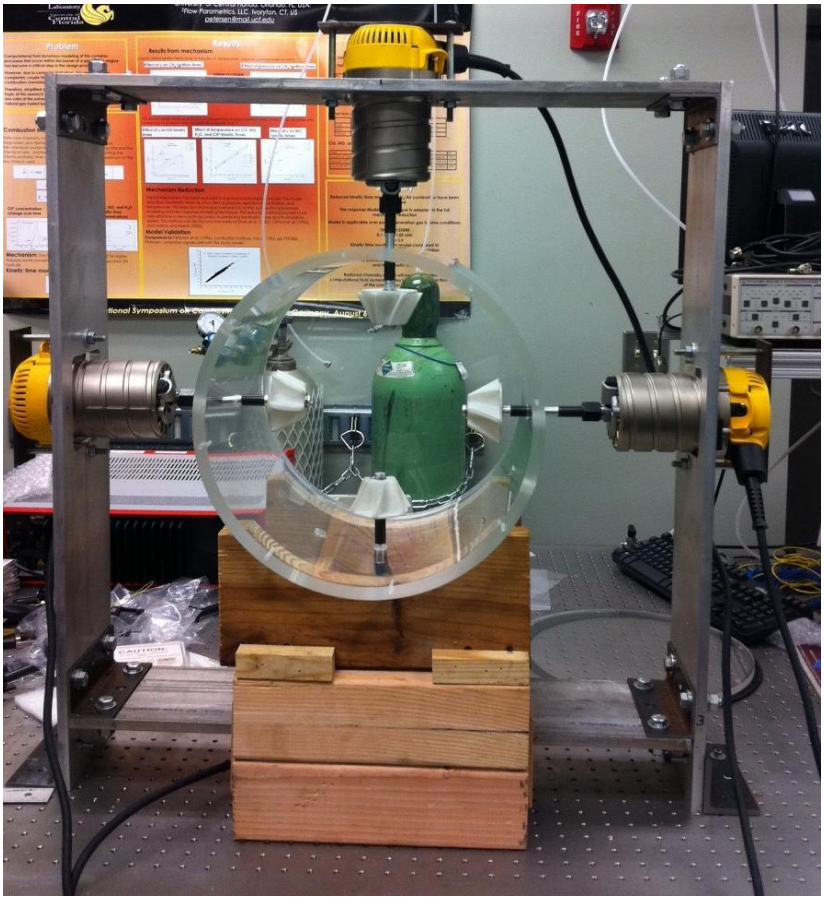

Fig. 4 Plexiglas vessel setup – front view.

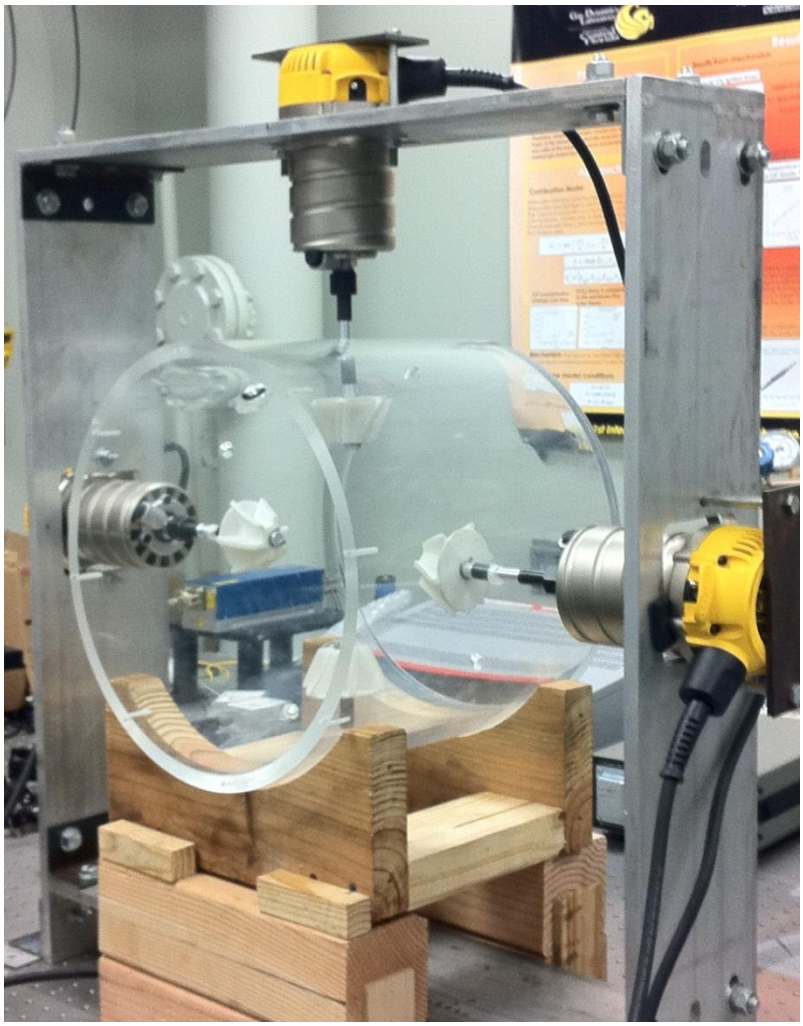

Fig. 5 Plexiglas vessel setup – side view.

During the fourth quarter of the effort, the initial characterization experiments were performed. The complete set of results as well as the final design for the turbulent flame speed setup will be presented in the fifth quarterly report.

TASK 3 – LAMINAR FLAME SPEED MEASUREMENTS WITH DILUENTS

The flame speed facility used in this study consists of two constant-volume cylindrical vessels. The first vessel is aerospace-grade aluminum and has an internal diameter of 30.5 cm with optical access using two fused quartz windows about 20 cm in diameter. This vessel is the facility's original flame speed bomb where more details about the vessel can be found in de Vries et al. (2011) and Lowry et al. (2011)0. The other vessel used in this study is a newly developed stainless steel vessel capable of performing experiments at initial temperatures up to 600 K and initial pressures up to 30 atm. The thick-walled vessel has an internal diameter of 31.8 cm and uses a similar optical access setup as the original flame speed facility which is discussed in Krejci et al. (2011).

The layout of the flame speed facility is shown in Fig. 6. Each vessel has its own thermocouple to monitor the initial gas mixture temperature. Each gas mixture is made using the partial-pressure method via 0–1000 Torr and 0–500 psi (34 atm) pressure transducers. Two additional pressure transducers with the same pressure capability are located near the stainless steel vessel to accurately monitor gas pressures at elevated temperatures. The purity of each gas used in this study is ultra-high purity grade, (≥ 99.9% for each primary gas). The filling and venting of gas mixtures are controlled remotely by electro-pneumatic valves. Additionally, the gas mixture is ignited remotely from a separate control room. The ignition consists of an adjustable, constant-current power supply, a 10-μF capacitor, an automotive coil, and a solenoid switch. The spark is created across two sharpened electrodes that are 0.9-mm (0.035 in) diameter Alloy X rods and are set at a variable gap.

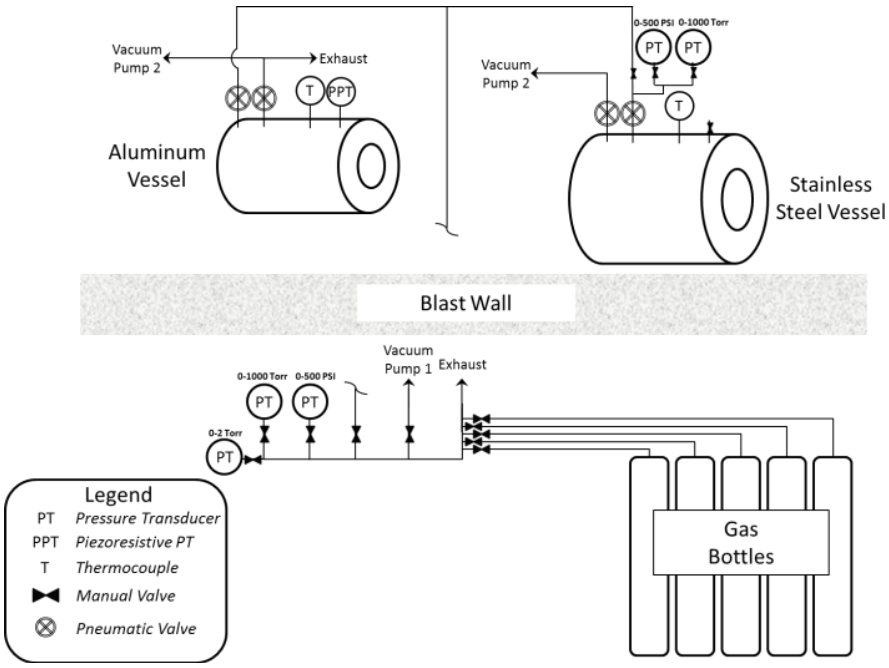

Fig. 6 Layout of the flame speed facility at Texas A&M University.

The experiment is visualized using a Z-type schlieren setup as suggest by Settles (2006)0. A schematic of the general optical setup is shown in Fig. 7. The source of light is generated by a

mercury arc lamp that is passed through a condenser lens before reflecting off the first 15.2 cm, f/8 parabolic mirror. The reflected light is passed through the vessel where it is reflected off a second 15.2-cm, f/8 parabolic mirror towards a high-speed camera. A circular pinhole aperture is used to cut off the light before entering the camera to intensify the density gradients as the flame spherically grows outwardly. The high-speed camera used to capture the event is a Photron FastCam SA 1.1. Example images from this study are shown in Fig. 8 to demonstrate the high quality-picture and the increase of flame instability with increasing pressure.

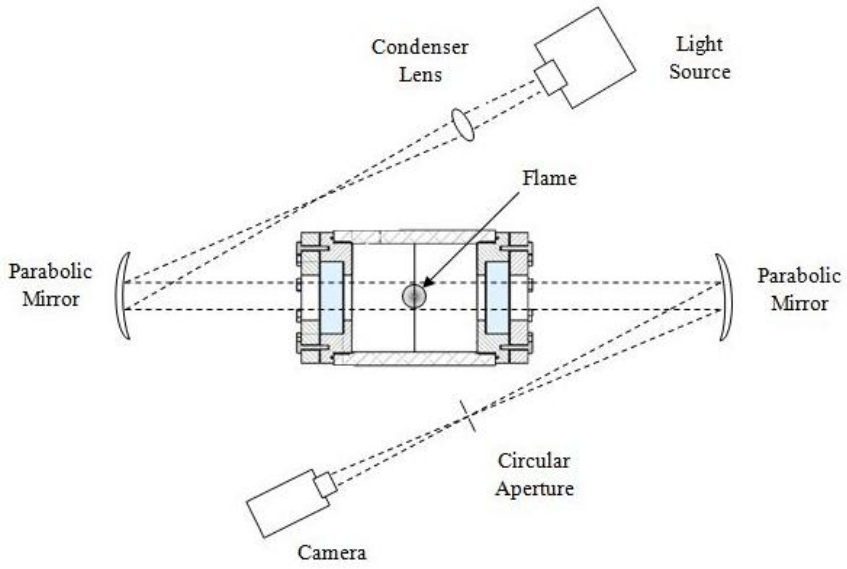

Fig. 7 Optical setup for high-speed schlieren system.

Data Analysis

After each experiment, the high-speed images are post processed using Matlab. A code has been developed and implemented to track the growth of the spherical flame in a similar manner as described by Lowry et al. (2011). Figure 9a shows a sample image of how the contrast of the image is changed so as to locate the outside edge of the flame, and Fig. 9b displays the original flame image with the flame edge detection and the six radial track points used to fit in a Euclidean circle algorithm.

The instantaneous flame radius given by the image post processing is analyzed using the linear relationship given by Eqns. 1-3 [Markstein, 1964; Dowdy et al., 1990; Brown et al., 1996].

$$S_b = S_b^o - L_{m,b}\alpha \tag{1}$$

Where S_b is the burned, stretched flame speed, S_b^o is the burned, un-stretched flame speed, $L_{m,b}$ is the burned Markstein Length and α is the flame stretch defined by

$$\alpha = \frac{1}{A}\frac{dA}{dt} = \frac{1}{4\pi R^2}\frac{d(4\pi R^2)}{dt} = \frac{2}{R}\frac{dR}{dt} \tag{2}$$

Equation 2 can be substituted into Eqn. 1 and integrated to result in Eqn. 3.

$$R = S_b^o \, t - 2L_{m,b} \, ln \, (R) + const \tag{3}$$

Where R is the instantaneous flame radius, and t is the corresponding time. Then the un-stretched flame speed and Markstein Length are obtained by using linear regression. The un-burned, un-stretched flame speed $S_{L,u}^o$ and Markstein Length $L_{m,u}$ are calculated by divided their respective burned values by the density ratio across the flame given by Eqn. 4.

$$\sigma = \frac{\rho_u}{\rho_b} \tag{4}$$

The density ratio is calculated using the authors' chemical kinetics model in Chemkin, using the STANJAN module [Reynolds, 1986].

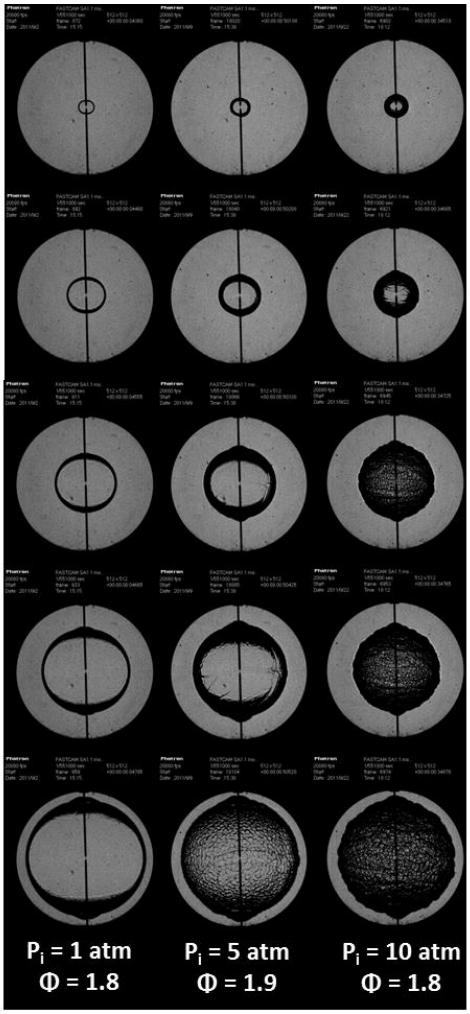

Fig. 8 Flame images for 1-atm (left), 5-atm (middle), and 10-atm (right) 50:50 H_2:CO. The oxidizer for the atmospheric experiment is air, while the oxidizer for the 5 and 10-atm experiments is 7:1 He:O_2.

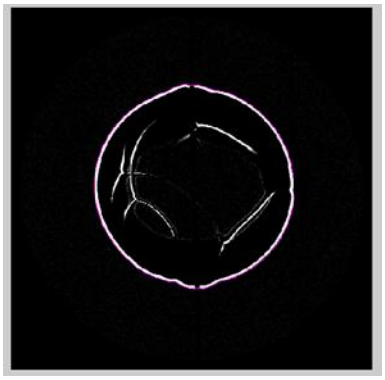

(a)

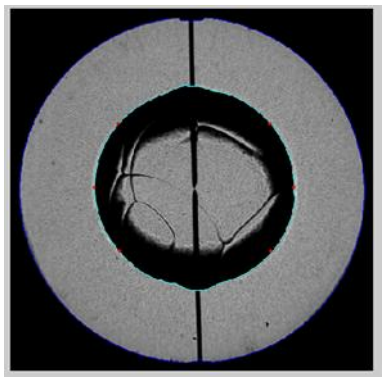

(b)

Fig. 9 Images from the flame detection program. (a) The contrast of the image is changed to locate the edge of the flame (b) The original image is shown with the edge detection.

Uncertainty Analysis

A brief overview of the uncertainty analysis is provided to demonstrate the repeatability for the experiments performed within this study. Systematic and random uncertainties were taken into account using the methods shown by Moffat (1988). The total experimental uncertainty, U_{S_L}, is given by Eqn. 5.

$$U_{S_L} = \sqrt{B_{S_L}^2 + \left(\frac{t_{M-1,95} S_{S_L}}{\sqrt{M}}\right)^2} \tag{5}$$

Where B_{S_L} is the total bias uncertainty, $t_{M-1,95}$ is the student *t* value at a 95% confidence interval and *M−1* degrees of freedom, S_{S_L} is the standard deviation of repeated experiments, and *M* is the number of repeated experiments per condition. The total bias uncertainty, shown by Eqn. 6, includes u_i, the fixed error for each variable x_i, and S_L, the relationship between the flame speed and each variable x_i.

$$B_{S_L} = \sqrt{\sum_{i=1}^{n} \left(\frac{\partial S_L(x_i)}{\partial x_i} u_i\right)^2} \tag{6}$$

A relationship between each independent variable and the flame speed must be known to use this definition of the total bias uncertainty. A correlation is developed similar to that shown in Lowry et al. (2011)0. Table 4 and Fig. 10 show a characteristic data set of the uncertainty analysis. The total uncertainty percentage demonstrates good predictability of the data.

Table 4 Atmospheric hydrogen flame speed uncertainty.

ϕ	$S^0_{L,u}$ (cm/s)	U_{SL} (cm/s)	%
0.5	67.2	7.1	10.6
0.6	96.5	7.3	7.6
0.7	124.4	7.3	5.9
0.8	169.9	7.2	4.2
0.9	194.0	6.9	3.6
1.0	218.0	7.2	3.3
1.1	236.7	7.1	3.0
1.2	254.9	7.3	2.8
1.3	267.4	7.4	2.8
1.4	275.0	7.2	2.6
1.5	280.3	7.1	2.5
1.6	282.8	7.2	2.5
1.7	283.8	7.4	2.6
1.8	282.9	7.2	2.5
1.9	280.3	7.1	2.5
2.0	278.9	6.9	2.5
2.5	249.1	6.9	2.8
3.0	217.4	6.9	3.2
3.5	187.6	6.9	3.7
4.0	158.7	6.9	4.4
4.5	133.0	6.9	5.2
5.0	110.1	6.9	6.3

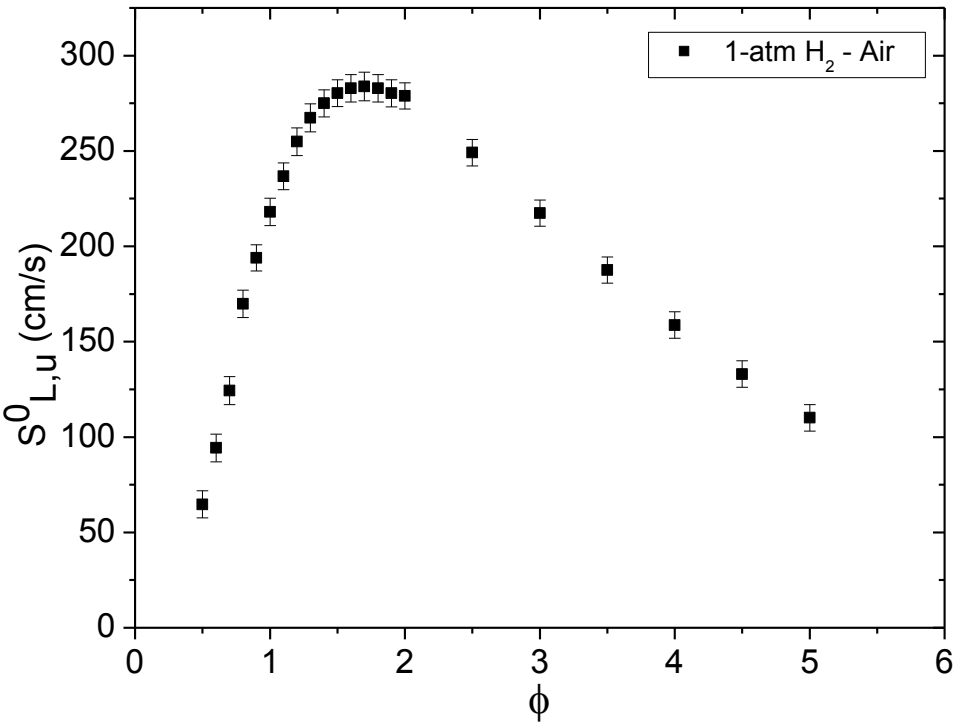

Fig. 10 Atmospheric hydrogen flame speed data with calculated uncertainty bars shown.

Computational Method

The detailed chemical kinetic mechanism utilized in this work is under constant development and optimization at the Combustion Chemistry Centre (NUI Galway). The $H_2/CO/O_2$ sub mechanism is based on the work of Ó Conaire et al. (2004) with several significant updates based on recent experimental and kinetic data. The changes are partially described in Kéromnès et al. (2011)0 and will be fully detailed in an upcoming publication.

Flame speed simulations were performed with the Premix module of Chemkin Pro (2010) using the multi-component transport equations. Solutions were converged to over 1000 grid points to essentially provide grid independent solutions. Shock-tube ignition delay simulations (see Tasks 4 and 6) were performed with the Aurora module assuming constant volume and constant energy conditions. Ignition delay time was defined as the time OH* reached 5% of its predicted maximum concentration. This definition essentially locates the onset of ignition, replicating well the experimental definition.

Results

This study includes experimental data from two gas dynamic experimental devices: constant-volume cylindrical bomb and high-pressure shock tube (see Tasks 4-6). The mixture compositions performed in the cylindrical bomb include hydrogen diluted with air at atmosphere pressure and three initial temperatures, hydrogen diluted with helium at two elevated pressures

and three temperatures, 50:50 H_2:CO diluted with air at 1 atm, and 50:50 H_2:CO diluted with helium at elevated pressures. For all elevated-pressure experiments, the oxidizer ratio was adjusted to a 7:1 He:O_2 ratio in order to increase the Lewis number of the mixtures and minimize hydrodynamic instabilities. Additionally, all initial temperatures have an uncertainty of ±3 K. Tables A1–A4 in the appendix provide the experimental results for all the conditions studied. Table 5 provides more details about the mixture compositions performed in this study for the laminar flame speeds.

Table 5 Experimental conditions for the cylindrical bomb measuring laminar flame speed.

H_2:CO	Temperature (K)	Pressure (atm)
100:0	298	1
		5
		10
	373	1
		5
	443	1
		5
50:50	298	1
		5
		10

Hydrogen. Figure 11 demonstrates an extensive literature comparison for atmospheric hydrogen-air at room temperature between the data herein and the experimental work done by Egolfopoulos and Law (1990); Vagelopoulos and Egolfopoulos (1994)0; Aung et al. (1997); Tse et al. (2000); Kwon et al. (2001)0; Lamoureux et al. (2003); Dahoe (2005); Verhelst et al. (2005)0; Burke et al. (2009)0; and Pareja et al. (2010). Since the H_2-O_2 chemical kinetic system has been well studied for the past few decades, it is expected that the agreement would be quite well between the data herein and previously published data, as shown in Fig. 11. However, unified agreement begins to dissipate at an equivalence ratio of about 1.0 and above. Additionally, when Fig. 11 is magnified to equivalence ratios below 1.0, as shown in Fig. 12, a potentially large variance exists amongst published flame speed data in a regime that typically has a distribution of about ±2 cm/s, such as the flame speed of methane-air 0Lowry et al., 2011]. The model exhibits excellent agreement with the new data of this study, reproducing it across the complete range of equivalence ratios. The model appears to slightly under predict the peak flame speed but is well within the experimental error bars depicted in Fig. 10.

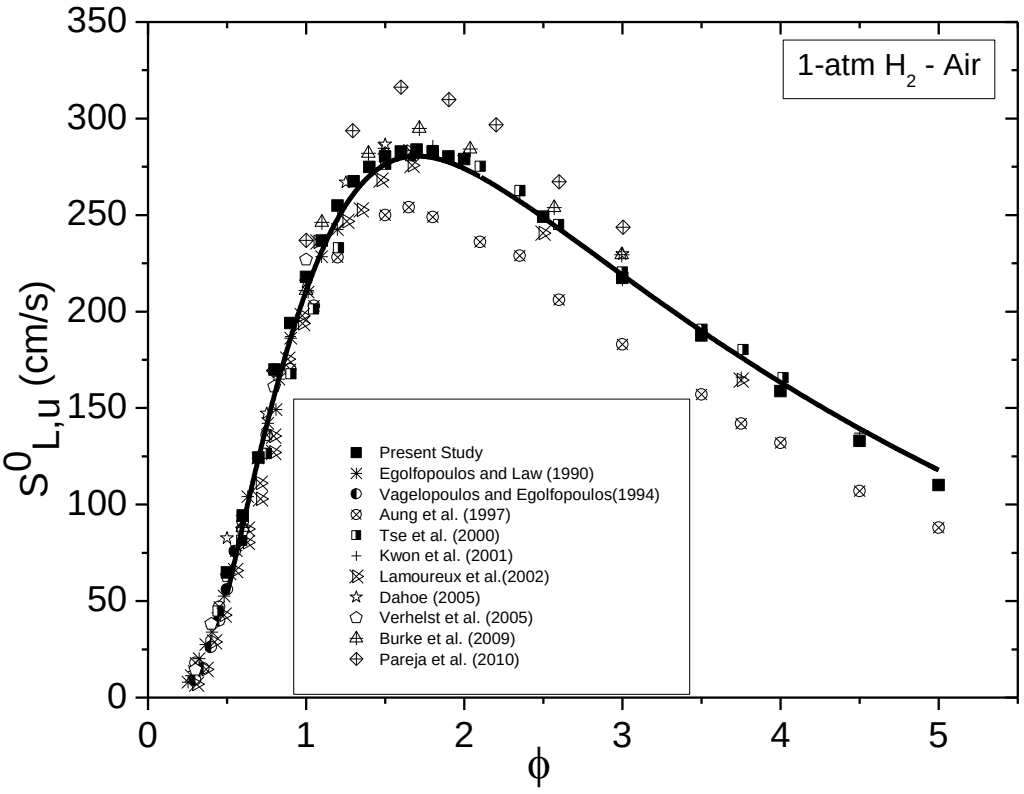

Fig. 11 Atmospheric hydrogen-air literature comparison to the data herein and the chemical kinetics model at standard temperature.

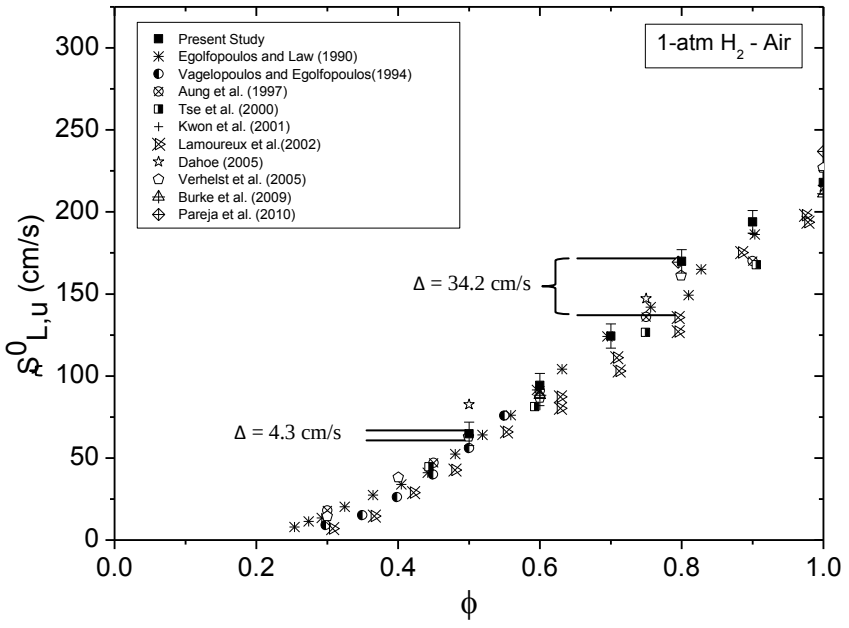

Fig. 12 Atmospheric hydrogen-air at equivalence ratios less than 1.0 demonstrating the increased distribution of laminar flame speed data.

Figure 13 explores the effects of pressure on hydrogen diluted with 7:1 $He:O_2$. With limited literature available at these pressures, this plot shows good agreement between the experimental data herein and data from Tse et al. (2000) at 5 atm. The model agrees quite well the 5 atm data obtained in this study, particularly under lean conditions and richer conditions ($\phi \geq 2$). However, the peak flame speed is underpredicted, with the model reproducing the existing data more accurately. The agreement deteriorates slightly with increasing pressure, with the model predicting a larger inhibiting effect of pressure than experimentally measured at an equivalence ratio around 1.5. Once again, the agreement at richer conditions is excellent.

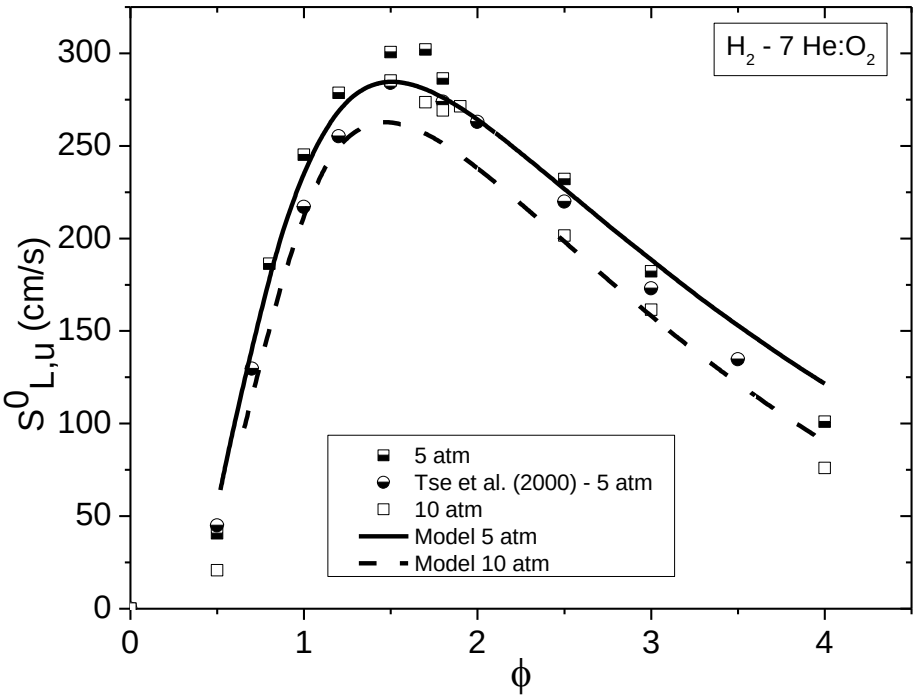

Fig. 13 Hydrogen diluted with $7He:O_2$ at 5 and 10 atm compared with the chemical kinetics model and data from Tse et al. (2000)0.

Figures 14 and 15 show the influence of initial pressures at elevated temperatures on the laminar flame speed. Hu et al. (2009) demonstrate excellent agreement for atmospheric hydrogen at elevated temperatures up to 443 K. Model agreement at 1 and 5 atm and elevated temperatures is excellent across the complete range of equivalence ratios.

Syngas. Figures 16 and 17 provide a baseline set of data for a common syngas (model) mixture with a 50:50 H_2/CO composition. The atmospheric syngas data herein, shown in Fig. 16, is compared with previously published data from McLean et al. (1994); Hassan et al. (1997)0; Sun et al. (2007)0; Natarajan et al. (2005); Burke et al. (2007)0; Prathap et al. (2008)0; Dong et al. (2009)0; and Bouvet et al. (2011)0. These data show a similar trend in agreement as seen with atmospheric hydrogen, where good agreement exists on the fuel-lean side, and discrepancies increase as the mixture becomes fuel rich. Once again, the model agreement with the data obtained in this study is excellent, with only minor disparities arising at high equivalence ratios.

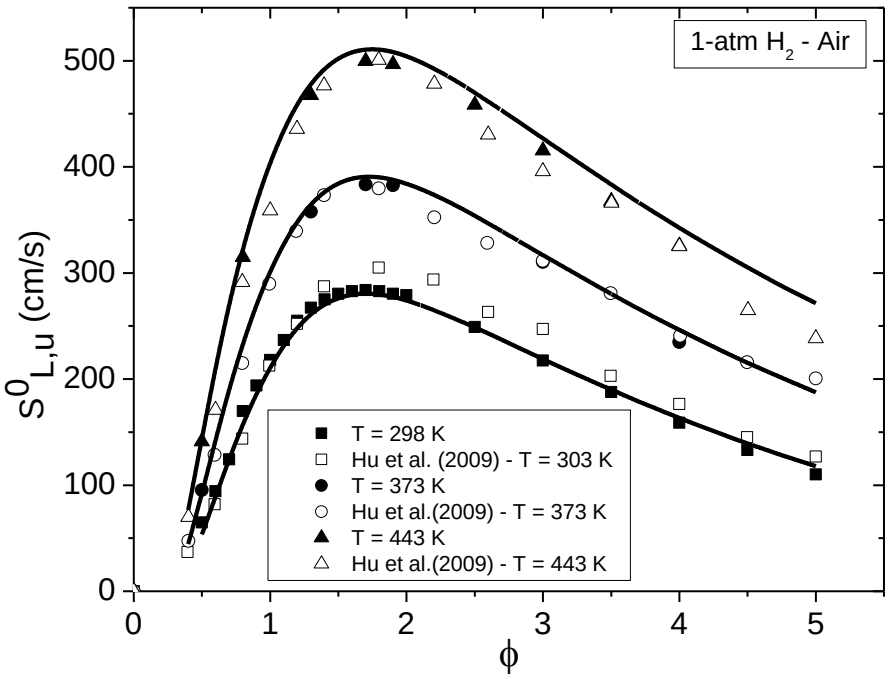

Fig. 14 Comparison of atmospheric hydrogen-air data herein, data from Hu et al. (2009)0, and the chemical kinetics model at elevated temperatures.

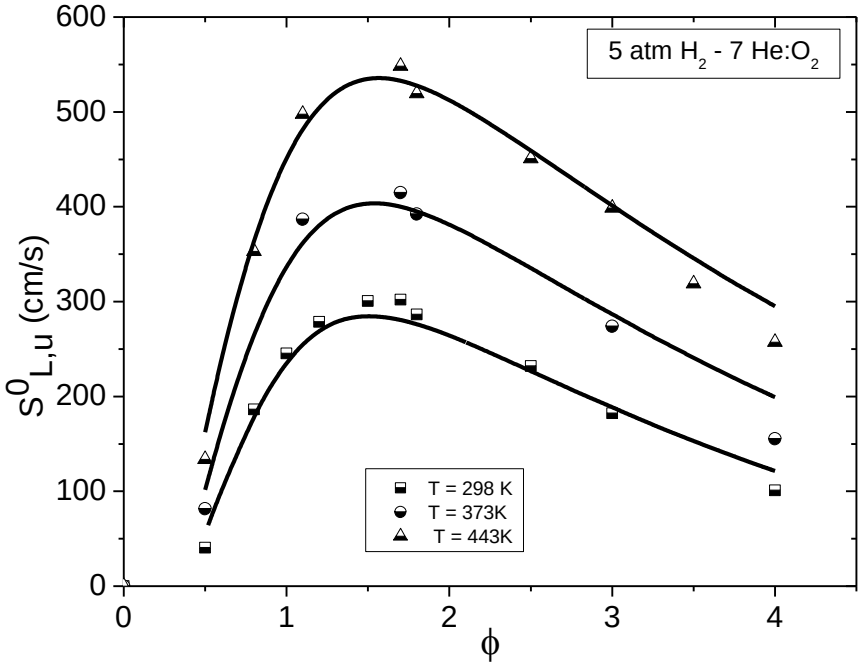

Fig. 15 Laminar flame speed of hydrogen diluted with 7:1 $He:O_2$ at 5 atm and elevated temperatures compared to the chemical kinetics model.

At elevated pressures, the 50:50 H_2:CO data herein are compared with Sun et al. (2007) and Natarajan et al. (2009) in Fig. 17. Overall agreement at both pressures is quite good. There are

some discrepancies around the peak flame speed at 10 atm which is under further investigation. This disagreement is also highlighted by the model, which predicts considerably lower reactivity at the elevated pressures, while reproducing the 5 atm data quite well.

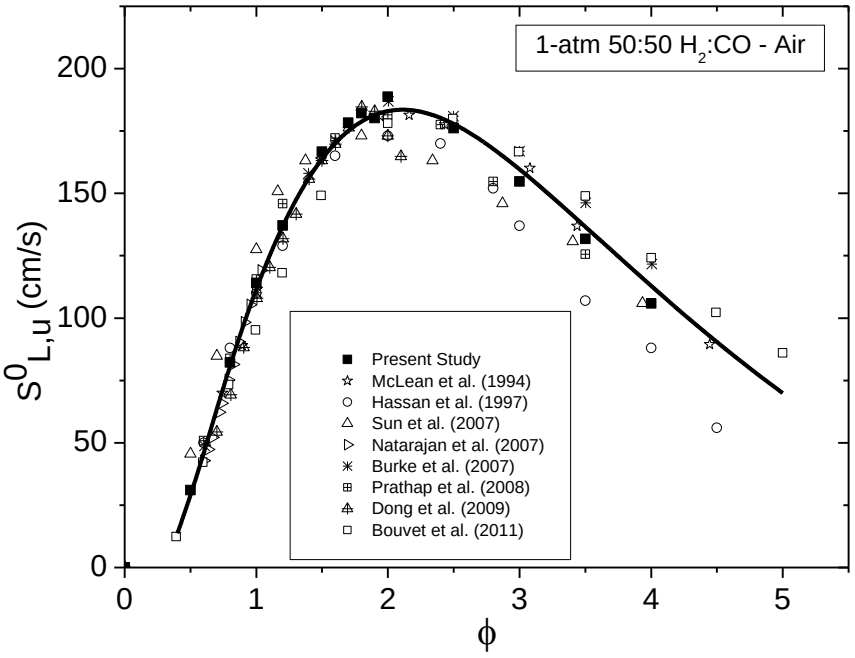

Fig. 16 Literature comparison of atmospheric 50:50 H_2:CO-Air with the data herein and the chemical kinetics model.

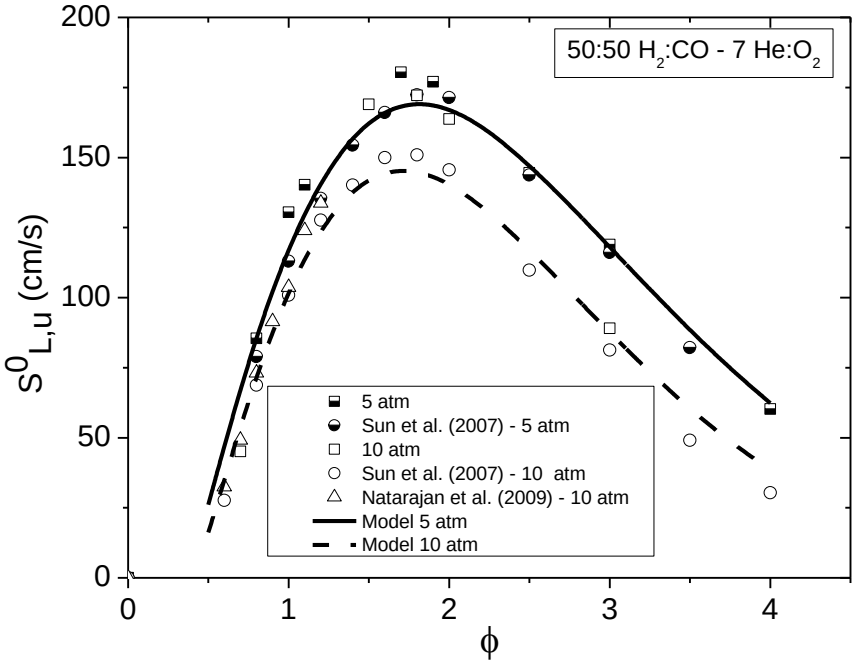

Fig. 17 Comparison of 5- and 10-atm 50:50 H_2:CO diluted with 7:1 He:O_2 with literature data and the chemical kinetics model.

TASK 4 – NOX MECHANISM VALIDATION EXPERIMENTS

For this task, a series of experiments is being conducted with the focus on shock-tube ignition delay times. Mixtures of hydrogen and oxygen as doped with levels of NO_2 (now) and N_2O (next quarter) to see measure the effect on the hydrogen oxidation chemistry. Such experiments are a good test of the kinetics mechanism, particularly the NOx kinetics mechanism. Pressures up to 30 atm are being performed to assess the effect of pressure on the NOx mechanism when combined with high-H_2 fuels.

The mixtures are highly diluted in argon (98%) so that gas dynamic effects are minimized. We can also avoid non-homogeneous effects that can arise in hydrogen mixtures at elevated pressures for more-concentrated fuel-oxidizer mixtures. Provided below are the experimental data for all the conditions conducted through the first year of this project.

Baseline experiments: H_2/O_2 mixtures

Equivalence ratio = 0.3 (0.75% H_2 + 1.25% O_2 in 98% Ar)

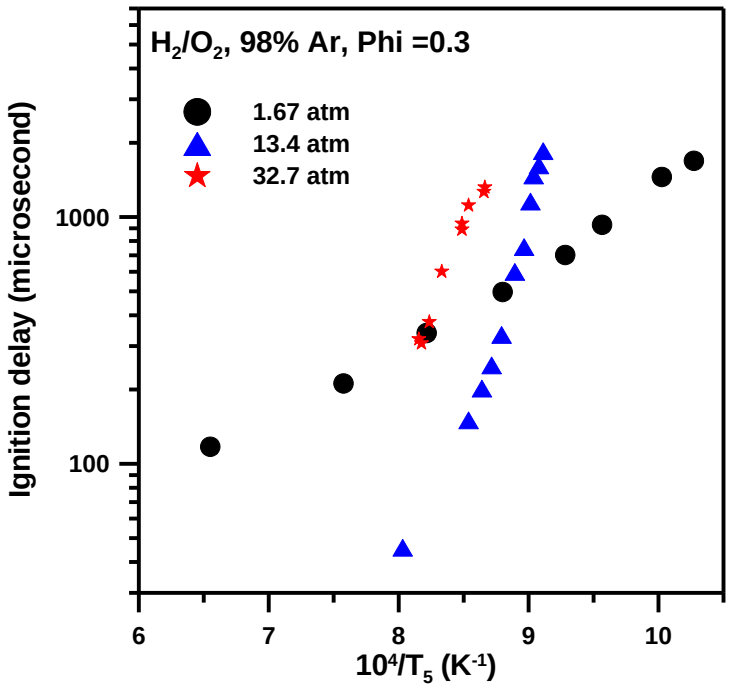

Fig. 18 Ignition delay times for mixtures of 0.75% H_2 + 1.25% O_2 in 98% Ar at average pressures of 1.67, 13.4 and 32.7 atm.

Equivalence ratio = 0.5 (1% H_2 + 1% O_2 in 98% Ar)

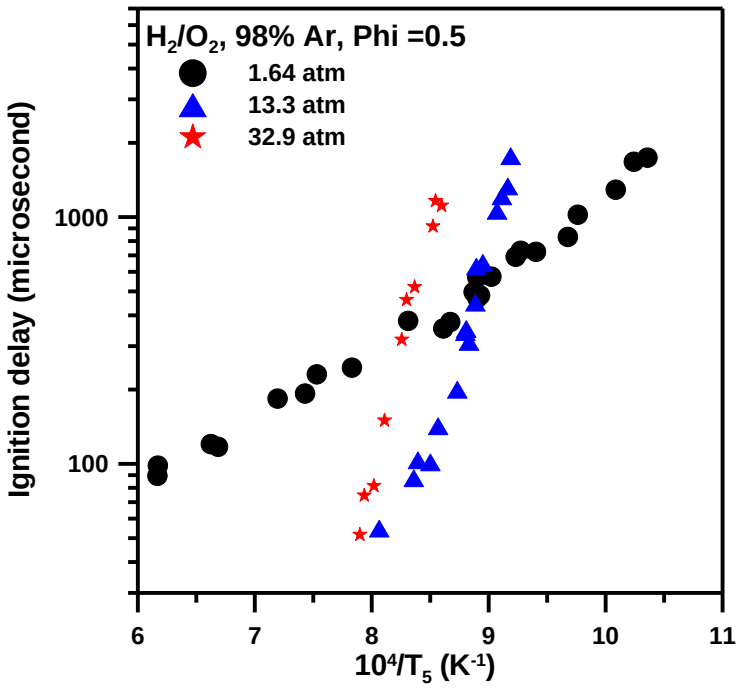

Fig. 19 Ignition delay times for mixtures of 1% H_2 + 1% O_2 in 98% Ar at average pressures of 1.64, 13.3 and 32.9 atm.

Equivalence ratio = 1.0 (1.33% H_2 + 0.67% O_2 in 98% Ar)

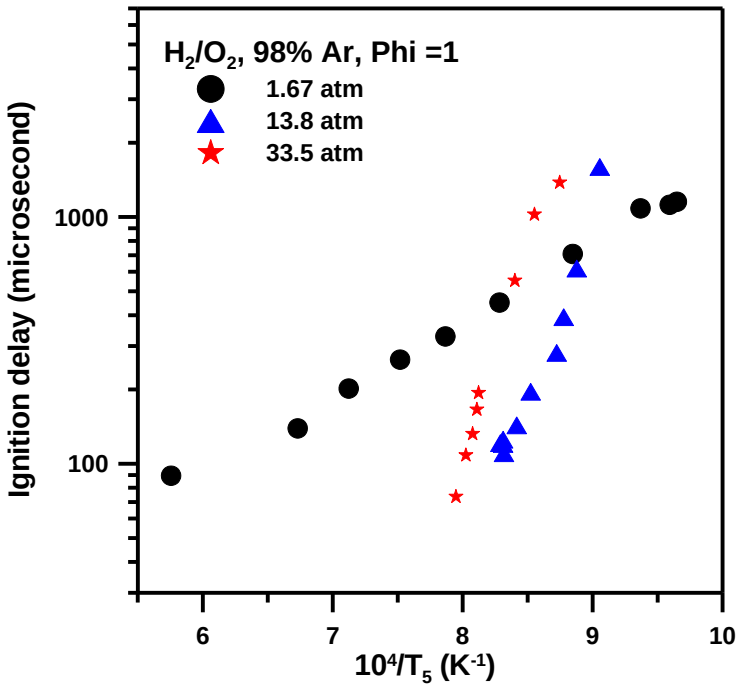

Fig. 20 Ignition delay times for mixtures of 1.33% H_2 + 0.67% O_2 in 98% Ar at average pressures of 1.67, 13.8 and 33.5 atm.

Effect of the equivalence ratio on the aut0 ignition delay of H_2/O_2 mixtures

Effect of the equivalence ratio on the auto ignition delay of H_2/O_2 mixtures around 1.65 atm

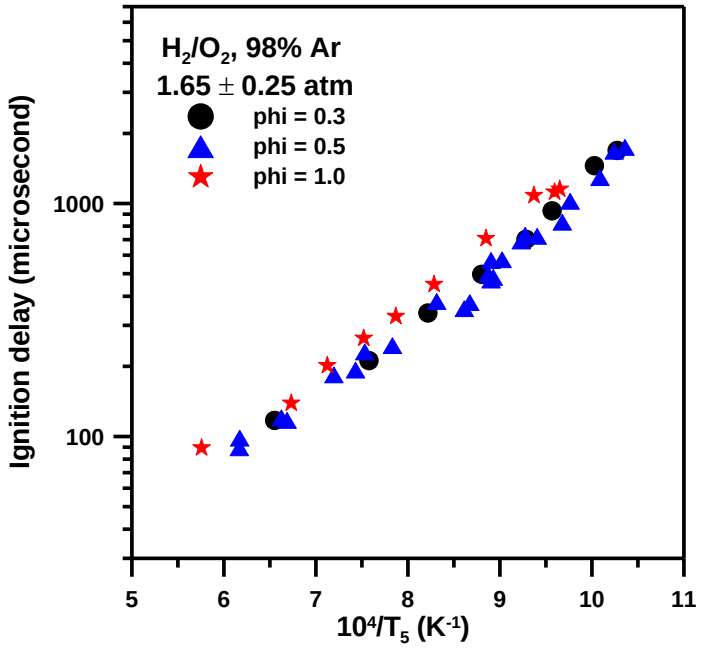

Fig. 21 Ignition delay times for various equivalence ratio of a H_2/O_2 mixture diluted in 98% Ar at an average pressure of 1.65 ± 0.25 atm.

Effect of the equivalence ratio on the auto ignition delay of H_2/O_2 mixtures around 13.5 atm

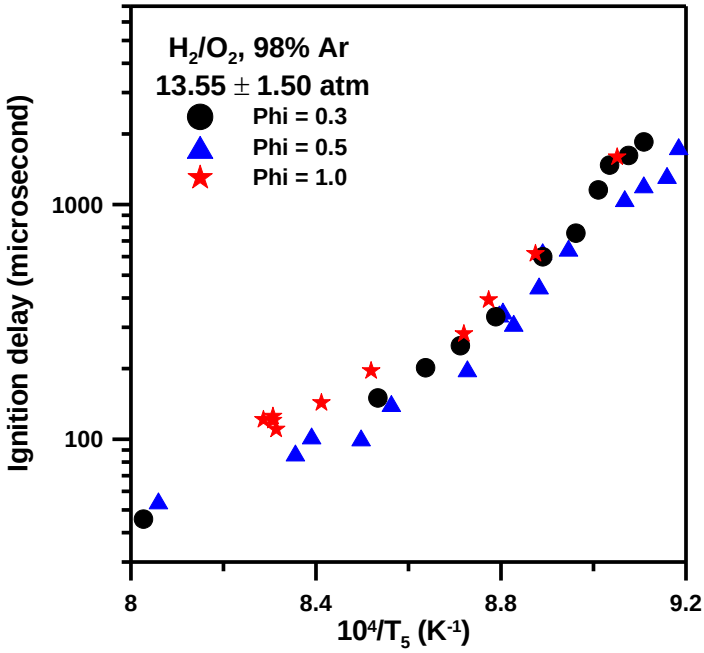

Fig. 22 Ignition delay times for various equivalence ratios of a H_2/O_2 mixture diluted in 98% Ar at an average pressure of 13.55 ± 1.5 atm.

Effect of the equivalence ratio on the auto ignition delay of H_2/O_2 mixtures around 33.0 atm

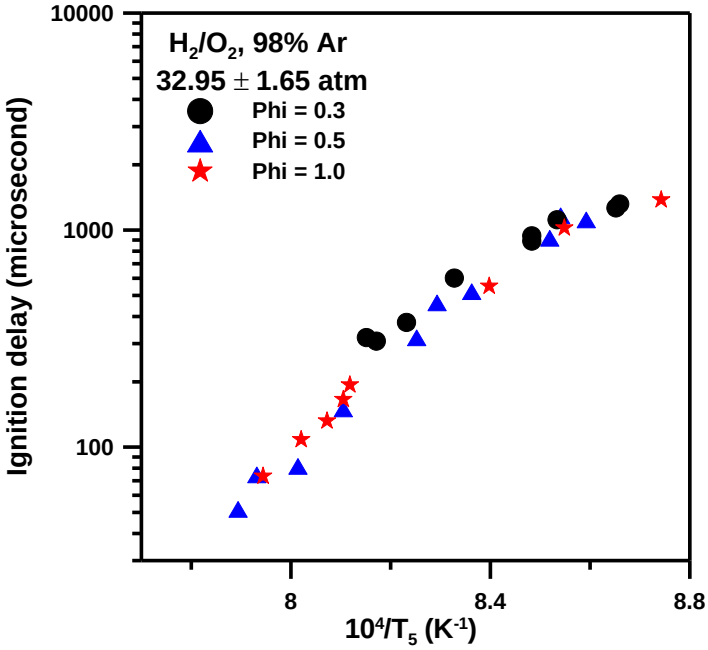

Fig. 23 Ignition delay times for various equivalence ratio of a H_2/O_2 mixture diluted in 98% Ar at an average pressure of 32.95 ± 1.65 atm.

Effect of NO_2 addition

Effect of an addition of 100 ppm of NO_2 on the ignition delay of H_2/O_2 mixtures

Equivalence ratio = 0.3 (0.75% H_2 + 1.25% O_2 + 100 ppm NO_2 in 97.99% Ar)

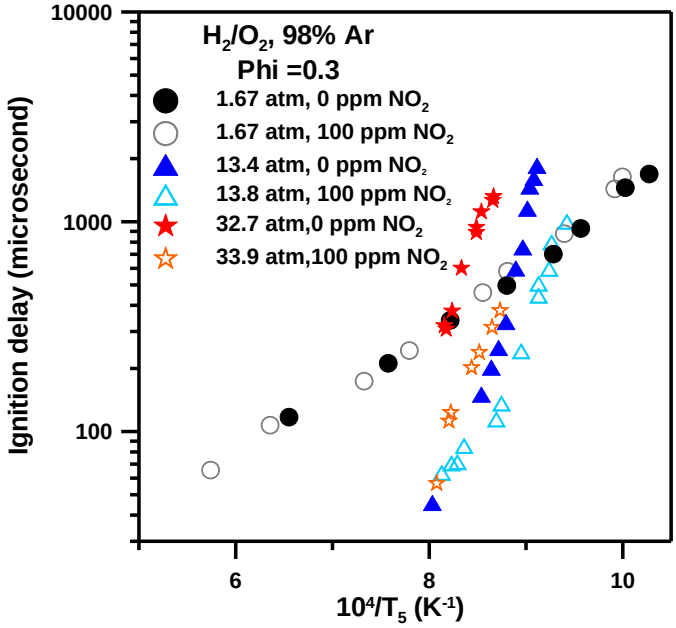

Fig. 24 Ignition delay times for mixtures of 1.33% H_2 + 0.67% O_2 in 98% Ar and 0.75% H_2 + 1.25% O_2 + 100 ppm NO_2 in 97.99% Ar around average pressures of 1.67, 13.6 and 33.3 atm.

Equivalence ratio = 0.5 (1% H_2 + 1% O_2 + 100 ppm NO_2 in 97.99% Ar)

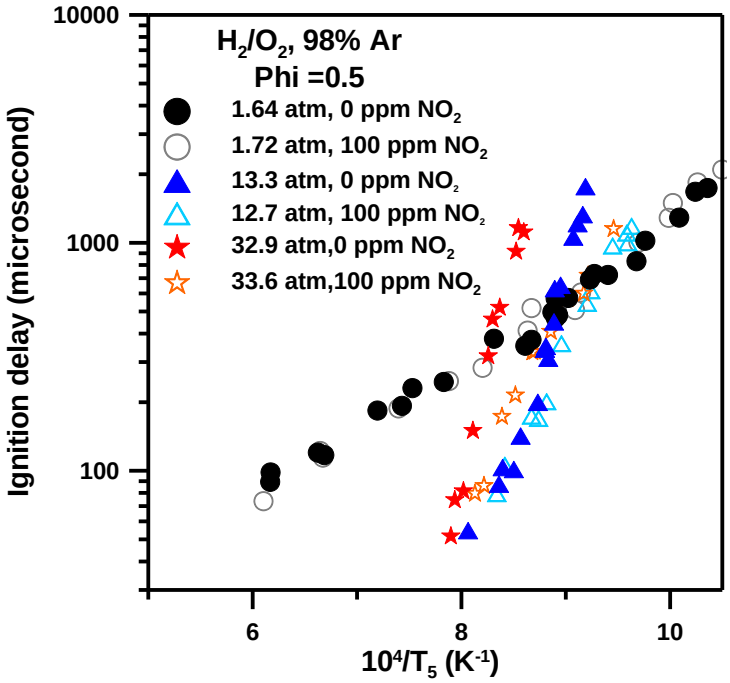

Fig. 25 Ignition delay times for mixtures of 1% H_2 + 1% O_2 in 98% Ar and 1% H_2 + 1% O_2 + 100 ppm NO_2 in 97.99% Ar around average pressures of 1.68, 13.0 and 33.3 atm.

Equivalence ratio = 1.0 (1.33% H_2 + 0.67% O_2 in 98% Ar)

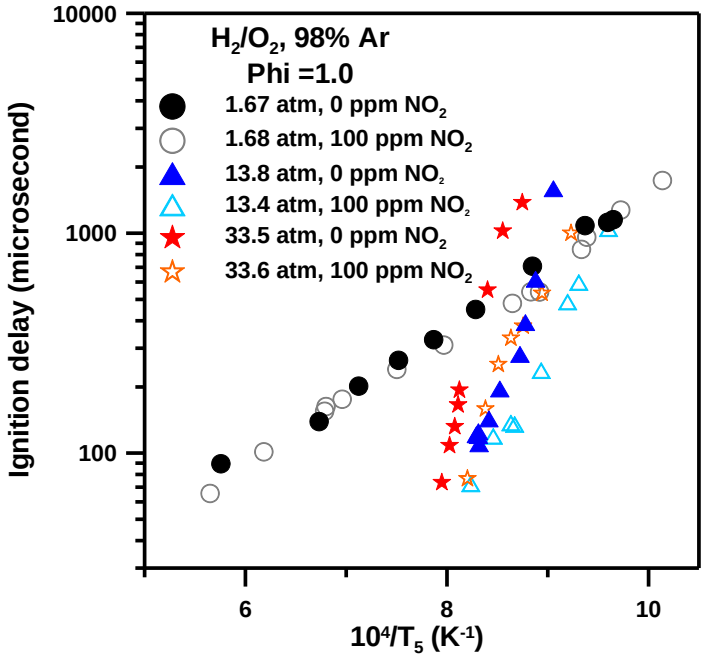

Fig. 26 Ignition delay times for mixtures of 1.33% H_2 + 0.67% O_2 in 98% Ar and 1.33% H_2 + 0.67% O_2 + 100 ppm NO_2 in 97.99% Ar around average pressures of 1.68, 13.6 and 33.6 atm.

Effect of the equivalence ratio on H_2/O_2/100 ppm NO_2 mixtures in 98% Ar

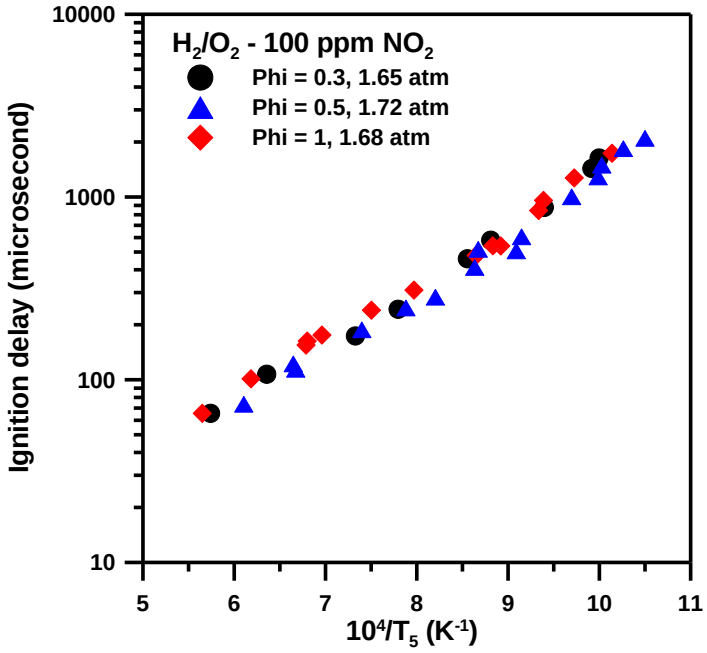

Fig. 27 Ignition delay times for various equivalence ratio of a H_2/O_2 mixture with 100 ppm NO_2 diluted in 97.99% Ar at an average pressure of 1.68 ± 0.04 atm.

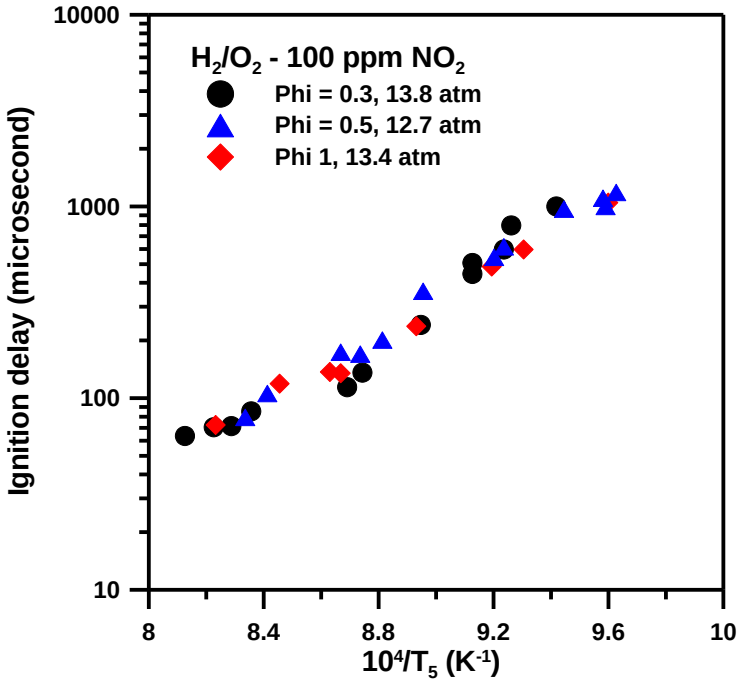

Fig. 28 Ignition delay time versus 1000/T (K) for various equivalence ratio of a H_2/O_2 mixture with 100 ppm NO_2 diluted in 97.99% Ar at an average pressure of 13.2 ± 0.5 atm.

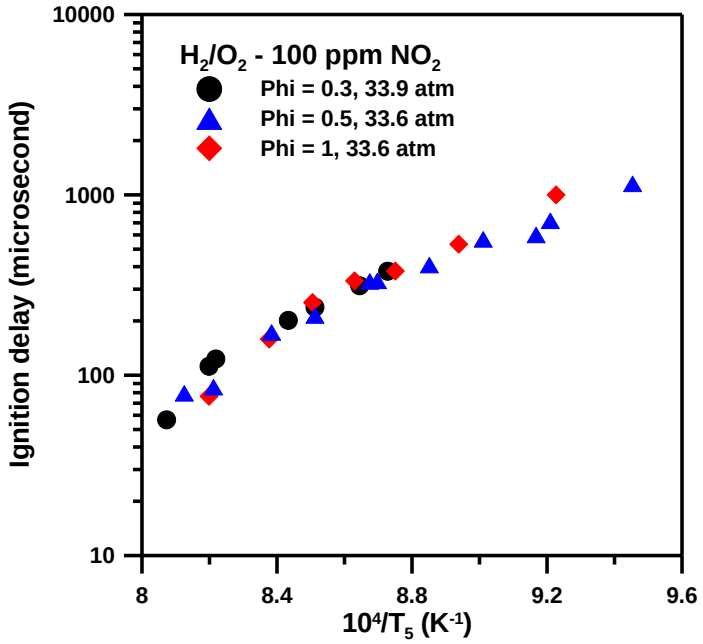

Fig. 29 Ignition delay times for various equivalence ratio of a H_2/O_2 mixture with 100 ppm NO_2 diluted in 97.99% Ar at an average pressure of 33.7 ± 0.2 atm.

Effect of the concentration of NO_2 on the ignition delay of H_2/O_2 mixtures diluted in Ar

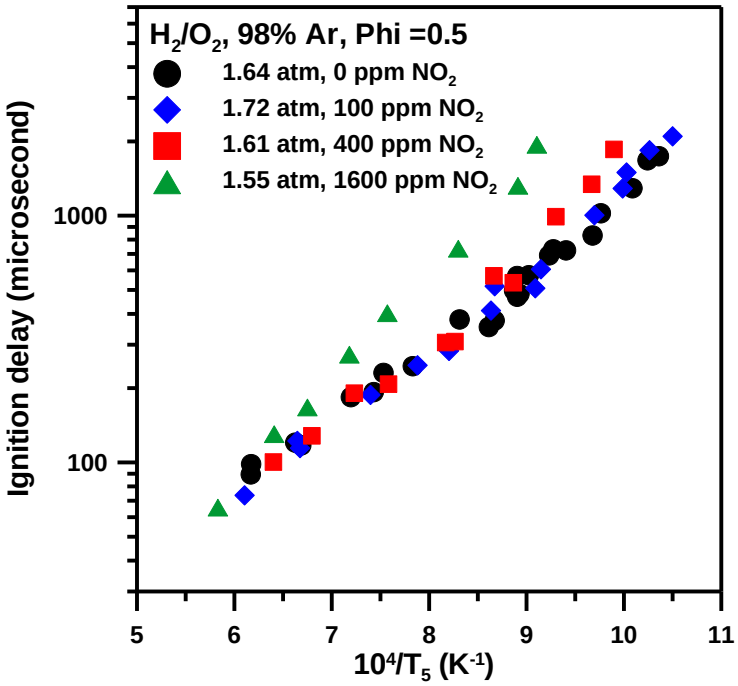

Fig. 30 Effect of various concentrations (0, 100, 400 and 1600 ppm) of NO_2 on the ignition delay time of H_2/O_2 mixtures at an equivalence ratio of 0.5 (1% O_2 +1% H_2) and diluted in, respectively, 98, 97.99, 97.96 and 97.84% Ar at an average pressure of 1.65 atm.

TASK 5 – FUNDAMENTAL NOX KINETICS

This task began during the second quarter. A review of the background literature on the NNH NOx mechanism was performed, a summary of which is provided as follows.

NNH Kinetics Background Research

Due to the importance of and increasing control of environmental regulations, the formation of nitrogen compounds and specifically NOx has received much attention in research for the past few decades. Several mechanisms have been developed to describe NOx formation during combustion. These mechanisms include the Thermal NO, Prompt NO, N_2O mechanism, fuel nitrogen, and the NNH mechanism. The NNH mechanism is the latest addition to the NOx formation mechanisms. This mechanism involves the creation of NNH through the reverse of the fast reaction:

(1) $$NNH \rightleftarrows H+N_2$$

Once NNH is created, it partakes in a bimolecular reaction with atomic oxygen to produce NO, through the reaction

(2) $$O+NNH \rightleftarrows NH+NO$$

The formation of NNH was originally proposed to be the dissociation of the adduct H_2NNO, which itself is produced by the reaction NH_2+NO. In the first work to propose the NNH mechanism, Bozzelli instead indicated that NNH is formed from the reverse of the dissociation reaction of NNH: $NNH \rightleftarrows H+N_2$ [Bozzelli and Dean, 1995]. The reverse of this reaction functioning to produce NNH is perhaps not intuitive due to the low barrier of the forward reaction (6-8 kcal/mol), and furthermore the forward reaction, the dissociation of NNH, is also enhanced by quantum tunneling. However, since tunneling is important to the forward reaction, it is also important in the reverse reaction. To produce NNH in amounts significant enough to be involved in bimolecular reactions, only a small concentration of H is required, due to the normally high concentration of N_2 in most combustion mixtures, and the large rate constant for equation (1). The small quantity of H needed to produce NNH is present in sufficient amounts during most combustion conditions.

Quantum tunneling is the process by which particles on the quantum scale cross an energy barrier that classical mechanics predicts is impossible. In this instance, quantum tunneling refers to the dissociation of NNH from the ground vibrational state, which is not at a high enough energy state to allow dissociation of the molecule. However, due to the uncertainty principle, NNH at the ground state may have enough energy to dissociate, giving the appearance to an observer that NNH "tunneled" to the energy required for dissociation.

Several rate constants were discussed by Bozzelli and Dean for reaction (1) in order to validate the rate constants that were used. The rate constants used were determined by theory, using the QRRK method. To further test the robustness of the rate constant, the activation energy was increased by a factor of 3. In doing this it was found that the rate constant was still better than other rate constants found in literature.

Once NNH is in partial equilibrium via reaction (1), the concentration of NNH is high enough to be involved in bimolecular reactions. The several species that could partake in a reaction with NNH are O_2, H, OH, and O. The possible reactions involving O_2 are:

(3) $$NNH+O_2 \rightleftarrows N_2+HO_2$$

(4) $$NNH+O_2 \rightleftarrows N_2O+OH$$

Both of these reactions are seemingly important due to the apparent very exothermic nature of reactions that remove hydrogen from a molecule. However, the rate constant for this reaction is actually quite slow. This behavior is due to the chemical process that must take place to make the products of the reaction, that is, an addition, isomerization, and elimination process must take place. The molecule HNNOO is first formed then undergoes isomerization to the molecule NNOOH, and lastly, the molecule splits into the products of reaction (4). This process is not a low entropic process as compared to other fast reactions. It therefore drives the reaction (4) to be a slow process.

The molecule NNH can also react with H to produce H_2 and N_2:

(5) $$NNH+H \rightleftarrows H_2+N_2$$

This reaction is significant, but the products are not of importance from a NOx production standpoint. In another reaction, NNH can combine with OH to form N_2 and H_2O:

(6) $$NNH+OH \rightleftarrows N_2+H_2O$$

This reaction, like reaction (5) does occur, but again it has little importance from a NOx production standpoint.

The molecule NNH, lastly, potentially interacts with O. This interaction has three possible reactions:

(7) $$O+NNH \rightleftarrows N_2+OH$$

(8) $$O+NNH \rightleftarrows N_2O+H$$

(9) $$O+NNH \rightleftarrows NH+NO$$

In these reactions, atomic oxygen combines with NNH to form the HNNO adduct. After the adduct is formed, each reaction undergoes a difference process. Reaction (7) undergoes an isomerization to NNOH, and then the products OH and N_2 are formed. Reaction (8), due to the low entropy of H, must absorb more energy than is present in the products, in order to break the HNNO adduct. Reaction (9) is the simplest, the N-N bond is broken and no isomerization or additional energy is needed to make the products. All three of these reactions, (7), (8), and (9), are exothermic. Reaction (7) is the most exothermic, reaction (8) is the second most exothermic and reaction (9) is the least exothermic. This would normally lead one to believe that reaction (7) would have the largest rate constant and (9) would have the lowest. However, due to the entropic effects of the additional processes that reactions (7) and (8) undergo, this leads to reaction (9)

having the largest rate constant. This is significant to NOx production, as can readily be seen by inspection of the products of reaction (9).

Since reactions (7) and (8) involve bimolecular reactions of NNH which do not produce NO, Bozzelli changed the estimates of the rate constants for reaction (7) and (8) to investigate this effect on NO production. Bozzelli found that NO concentrations were unchanged. This fact illustrates that NNH production in reaction (1) is very fast. Even though NNH is being used in other reactions which do not produce NO, the pool of NNH available to participate in reaction (9) effectively remains unchanged due to the speed that reaction (1) replenishes NNH concentration.

In order to function, the NNH mechanism needs a significant concentration of atomic oxygen and only a small concentration of H atoms, due to the speed of reaction (1). This indicates that more NO production occurs at lower temperatures than would be predicted by the Zeldovich mechanism alone. As a result of the NNH mechanism, NO production is more significant in H_2 flames since the Prompt NO mechanism cannot function to produce NO without the presence of hydrocarbon radicals.

Bozzelli and Dean (1995) proposed an interesting consequence of the NNH mechanism. Due to the need for the NNH mechanism to have atomic hydrogen present, the concentration of H available to partake in other reactions is diminished, or at least changed. This affects the kinetics of Thermal DeNOx as Thermal DeNOx uses atomic hydrogen to remove NOx. The temperature window in which Thermal DeNOx is active is 1100-1200 K, already a small window. As mentioned in the previous paragraph, the NNH mechanism plays a larger role in NO formation at lower temperatures. Bozzelli calculated that the NNH mechanism counteracts Thermal DeNOx in the bottom portion of its window, reducing the window by approximately 20 K, i.e. the new window would be 1120-1200 K. It is unknown if this change in the effective temperature range of Thermal DeNox is experimentally verifiable, however, the potential for the NNH mechanism to further increase NO production through reducing the effectiveness of NO reducing mechanism is worthy of note.

In the Bozzelli and Dean reference (1995), other radicals were analyzed which could interact with N_2, producing an adduct that could react with O and then form NO. Bozzelli and Dean analyzed N_2 combining with OH and with CH_3. Both of the adducts formed here, NNOH and CH_3NN, have equilibrium concentrations that are too small to be significant in a bimolecular reaction with O to form NO.

In work done by Konnov and De Ruyck (2001), experiments were conducted to verify the rate constant of reaction (9). The rate constant for reaction (9) was calculated by Bozzelli and Dean to be 7×10^{13} cm^3/mol/s. Konnov and De Ruyck confirmed this calculated rate constant. However, in experiments conducted to measure NO concentration in hydrogen flames, the rate constant for reaction (9) was shown to be 4×10^{13} cm^3/mol/s. Konnov and De Ruyck (2001) also proposed a new route for NO production in the NNH mechanism. In this proposed new route, after reaction (1), the following reactions occur:

(10) $$NNH+H+M \rightleftarrows N_2H_2+M$$

(11) $N_2H_2+H+M \rightleftarrows N_2H_3+M$

(12) $N_2H_3+H_2 \rightleftarrows NH_3+ NH_2$

After this, NH_3 and NH_2 and are oxidized to NO via the sequence: $NH_3 \rightarrow NH_2 \rightarrow NH \rightarrow N \rightarrow NO$. This new N_2H_3-route for NO production as part of the NNH mechanism has not been confirmed. Konnov and De Ruyck (2001) do provide substantiation for this new route. It was shown that predicted NO concentration had better agreement with experiments when the N_2H_3-route was included in the mechanism.

Experiments

During this period, much progress was made toward preparing the laser absorption diagnostic for experiments in the shock tube. The target species will be NH, with has a known spectroscopic transition in the ultraviolet. The basic laser setup being employed is shown in Fig. 31. It consists of a tunable ring-dye laser that is pumped by a green diode laser. The visible output from the ring dye laser is sent to an external frequency-doubling component (containing the doubling crystal) which converts the visible light to the target uv light. The laser is located at the laboratory at The Aerospace Corporation. To get the system on line and to train the TAMU student on the operation of this complex system, laser light near 306 nm is the first goal, corresponding to the OH molecule. We anticipate the first laser absorption experiments in a hydrogen system to be performed in the following quarter, with a goal toward moving to the NH wavelength by the end of Q4.

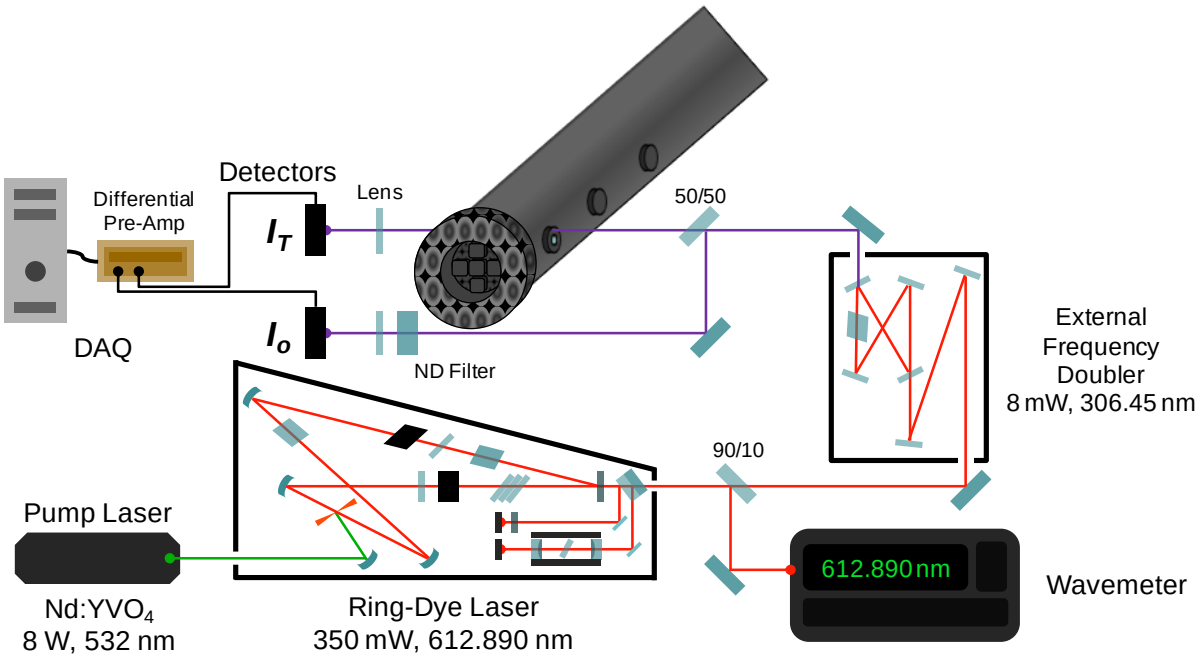

Fig. 31 Ring dye laser-based absorption setup being implemented in the present experiments. The laser is frequency doubled into the uv, where the NH transition can be found. Current setup is targeting OH at 306 nm for setup of the overall system and for training the graduate student.

TASK 6 – EFFECT OF IMPURITIES ON SYNGAS KINETICS

A detailed summary of the background work and the selection of mixtures for this task were provided in the third quarterly report. Provided below is a summary of the recent shock-tube experiments, primarily those associated with the baseline hydrogen and syngas mixtures to which the future impurity studies will be compared.

Shock-Tube Experiments

Ignition delay time, τ_{ign}, measurements were conducted in a single-diaphragm, stainless steel shock tube. The driven section is 4.72 m long with an internal diameter of 15.24 cm, and the driver section is 2.46-m long with an internal diameter of 7.62 cm. A 1.27-cm wall thickness allows for pressure behind reflected shock waves, P_5, up to 100 atm. The driven section is weld less with an inside surface polish of 1 μm root mean square roughness (RMS) or better. The speed of the shock wave is measured through five, equally spaced PCB P113A piezoelectric pressure transducers mounted flush with the inner surface of the driven section. The signals delivered by these five pressure transducers are sent to four Fluke PM-6666 counter boxes which record the time for the shock wave to travel from one transducer to the next; therefore, the shock wave velocity can be determined. These four velocities are then curve fitted to give the incident wave speed at the endwall location. Post reflected-shock conditions are obtained by using this incident wave speed in conjunction with one-dimensional shock relations and the initial conditions at the test region. This method was proven to maintain the uncertainty on the temperature determination behind reflected shock waves, T_5, below 10 K [Petersen et al., 2005]. Test pressure is monitored by one PCB 134A located at the endwall and one Kistler 603 B1 located at the sidewall. The observation window, located in the same plane as the pressure transducers on the endwall and sidewall, is made of CaF_2 and is located 16 mm from the endwall.

Experiments were performed at three different pressure conditions, 1.5, 12, and 30 atm, at an equivalence ratio, ϕ, of 0.5. Polycarbonate diaphragms, 0.25-mm and 2×1.02-mm thickness, were used for test pressures of 1.5 and 12 atm, respectively, and pre-scored aluminum diaphragms, 2.29-mm thickness, were used for the 30-atm experiments. A cross-shaped cutter was employed to facilitate breakage of the polycarbonate diaphragms to prevent fragments from tearing off. The driver gas used in this study was helium.

Prior to every run, the driven section was vacuumed down to 2×10^{-5} Torr or better using a roughing pump and a Varian 551 Turbo-molecular pump. The pumping time between experiments was minimized using a pneumatically driven poppet valve matching the inside diameter of the driven section and allowing for a passage of 7.62-cm diameter of gas between the vacuum section and the driven tube. The pressure was measured using a 0-10 Torr and a 0-1000 Torr MKS Baratron model 626A capacitance manometers and an ion gauge for the higher vacuums.

Test mixtures were prepared manometrically into a mixing tank of 3.05-m length made from stainless steel tubing with an inner diameter of 15.24 cm. The pressure in the mixing tank was measured using 0–17-atm Setra GCT-225 pressure transducers. The mixing tank is connected to the vacuum system and can be pumped down to pressures below 1×10^{-6} Torr. The gases (H_2

(Praxair, 99.999%), O_2 (Praxair, 99.999%), CO (Praxair 99.9%) and Ar (Acetylene Oxygen Company, 99.999%)) entering the mixing tank were passed through a perforated stinger in the center of the mixing tank to allow for turbulent mixing. To further ensured homogeneity through diffusion processes, mixtures are allowed to rest for at least 45 minutes prior to the first experiment. To minimize the potential formation of $FeCO_5$, which has a potential inhibitor effect on flames [Bouvet et al., 2011]0, the gas cylinder for the carbon monoxide is made of aluminum and the gas supply tubing was made of Teflon (for both the shock-tube and flame speed experiments).

Data Analysis

Ignition delay time was measured using the emission spectroscopy from the $A^2\Sigma^+ \rightarrow X^2\Pi$ transition of the excited-state hydroxyl radical (OH*) using an interference filter centered at 307 ± 10 nm with a Hamamatsu 1P21 photomultiplier tube. The ignition delay time is defined as the time between the passage of the reflected shock wave, indicated by a pressure jump in the signal delivered by the sidewall pressure transducer, and the intersection of lines drawn along the steepest rate-of-change of OH* de-excitation and a horizontal which defines the zero-concentration level, shown in Fig. 32. All of the data signals were processed through a 14-bit GageScope digital oscilloscope with sampling rates of 1 MHz or greater per channel.

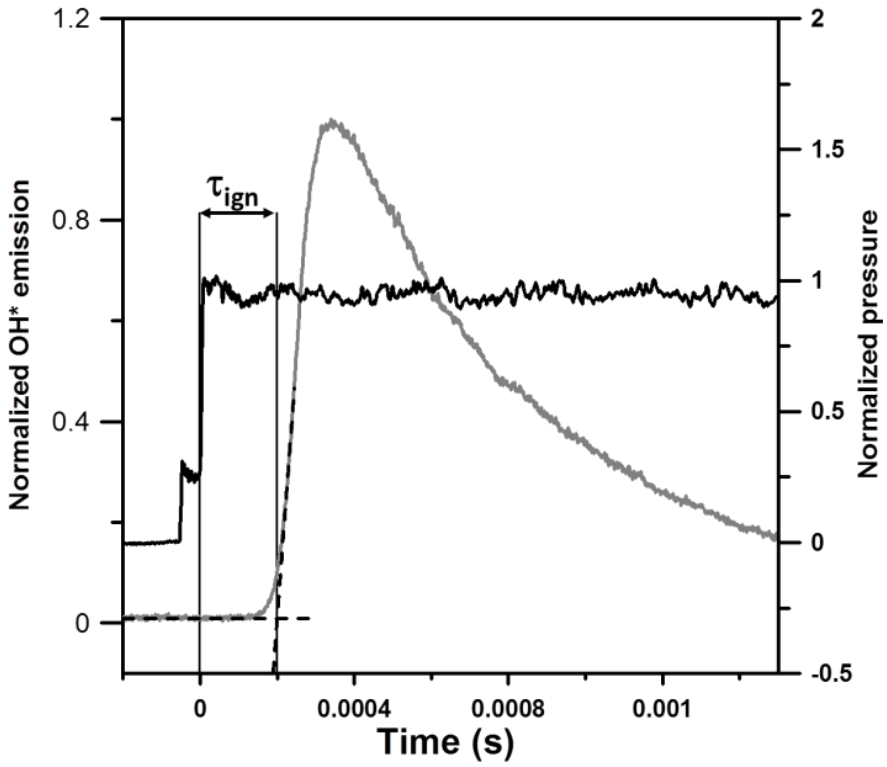

Fig. 32 Determination of the ignition delay time from normalized OH* (grey) and pressure (black) profiles with a mixture of 0.5% H_2 + 0.5% CO + 1% O_2 in 98% Ar at 1375 K and 1.65 atm.

There are two main uncertainties in the measured ignition delay times. The most important one is in the determination of the temperature behind the reflected shock wave. As mentioned earlier, the experimental setup and method used allow for a determination of T_5 with less than 10-K uncertainty. This uncertainty on T_5 can lead to a relatively important uncertainty in the ignition delay time for the high-pressure conditions of this study. The second source of uncertainty corresponds to the determination of the steepest rate of change from the OH* de-excitation profile. However, this uncertainty is smaller than the uncertainty on T_5. Overall, the total uncertainty on τ_{ign} reported in this study is between 10% at low pressure and 20% at 30 atm.

Results

The experiments performed on the high-pressure shock tube swept various compositions of hydrogen and carbon monoxide at three pressures and several temperatures. Table 6 provides more details about the mixture compositions performed in this study using the shock-tube facility.

Table 6 Experimental conditions for the shock-tube study of various H_2/CO mixtures at ϕ = 0.5 diluted in 98% Ar.

Mixture Composition (molar fraction) in 98% Ar	**T_5 (K)**	**P_5 (atm)**
0.01 H_2/0.01 O_2	960 - 1625	1.65 ± 0.15
	1085 - 1245	13.3 ± 1.0
	1160 - 1270	32.8 ± 1.5
0.002 CO/0.008 H_2/0.01 O_2	980 - 1705	1.65 ± 0.15
	1095 - 1300	12.3 ± 0.5
	1180 - 1265	31.3 ± 1.0
0.005 CO/0.005 H_2/0.01 O_2	990 - 2000	1.65 ± 0.21
	1095 - 1385	11.9 ± 0.7
	1170 - 1330	32.3 ± 0.5
0.006 CO/0.004 H_2/0.01 O_2	1015 - 1845	1.73 ± 0.21
	1090 - 1440	12.5 ± 0.8
	1140 - 1300	31.3 ± 0.7
0.008 CO/0.002 H_2/0.01 O_2	1055 - 1925	1.64 ± 0.27
	1095 - 1390	12.4 ± 0.6
	1175 - 1320	31.3 ± 0.8
0.009 CO/0.001 H_2/0.01 O_2	1025 - 1975	1.59 ± 0.18
	1115 - 1390	12.0 ± 0.9
	1160 - 1330	31.3 ± 1.0

The effect of the CO concentration on τ_{ign} can be better visualized by comparing the data to H_2/O_2 results acquired under similar conditions during a recent study. As can be seen in Figs. 33, 34, and 35, addition of CO leads to an increase in the ignition delay time at the different test pressures. However, this increase seems to be pressure dependent. Figure 33 shows that τ_{ign} increases with increasing amount of carbon monoxide on the full-scale range of tested temperatures. However Figs. 34 and 35, where the pressure is 12 and 32 atm, respectively,

demonstrate that the τ_{ign} are very similar at low temperatures. Additionally, it is worth noting that at high temperatures the increase in the τ_{ign} with increasing carbon monoxide is proportionally more important for pressures around 12 and 30 atm than at 1.6 atm.

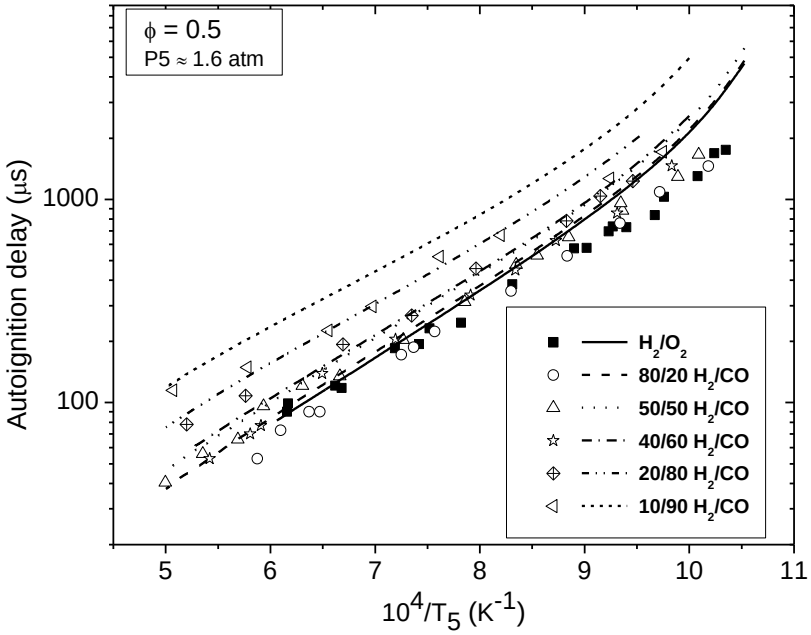

Fig. 33 Evolution of the ignition delay time with the inverse of the temperature at around 1.6 atm for various mixtures of $H_2/CO/O_2$ (98% dilution in Ar, $\phi = 0.5$). Lines are model simulations.

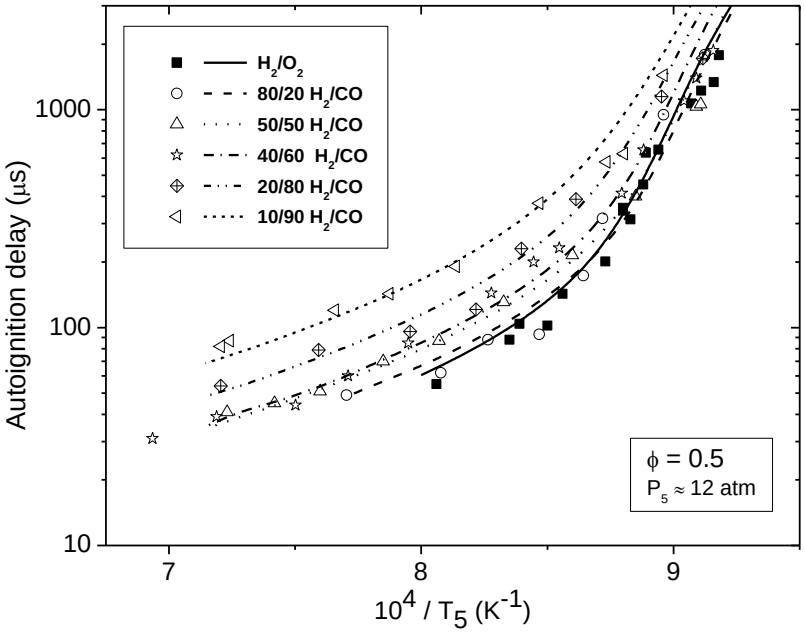

Fig. 34 Evolution of the ignition delay time with the inverse of the temperature at around 12 atm for various mixtures of $H_2/CO/O_2$ (98% dilution in Ar, $\phi = 0.5$). Lines are model simulations.

As can be seen from Figures 33–35, there are no distinguishable differences between the results obtained with H_2 and with those obtained with the 80:20 H_2:CO mixture. For higher carbon monoxide proportions however, an increase in τ_{ign} is observable. When the fuel composition is above 60% CO, the effects on τ_{ign} are amplified and are clearly visible. For 12 atm and above, the increase in the delay becomes very important at high temperatures, and even a slight increase of τ_{ign} can be observed at low temperatures with the 10:90 H_2:CO mixture. Also note that the differences between the 50 and 60% carbon monoxide fuel is very small compared to the differences between 80 and 90% carbon monoxide fuel.

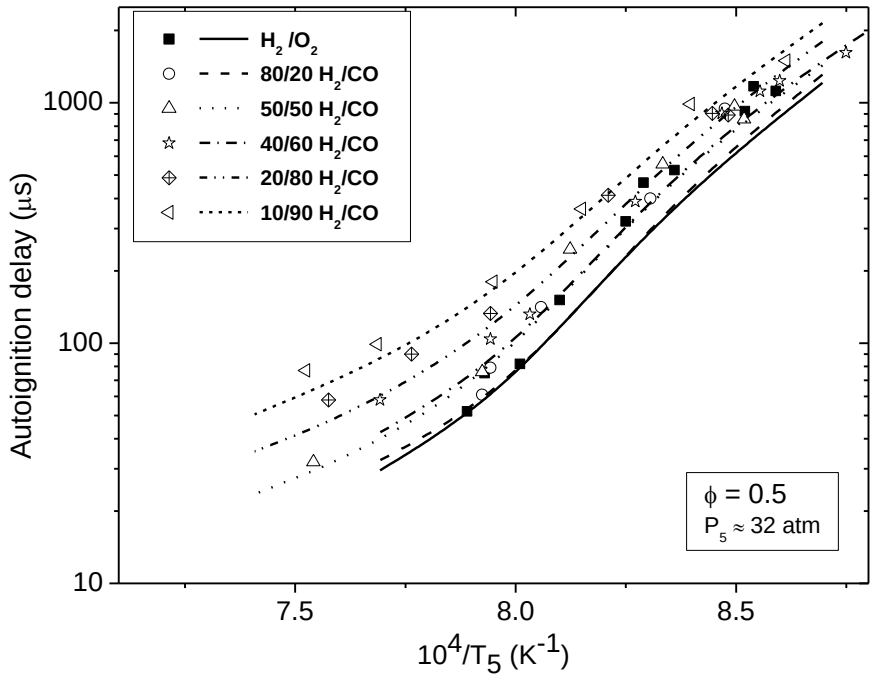

Fig. 35 Evolution of the ignition delay time with the inverse of the temperature at around 30 atm for various mixtures of H_2/CO/O_2 98% (dilution in Ar, ϕ = 0.5). Lines are model simulations.

The effect of carbon monoxide addition is well predicted by the model, particularly at the higher pressures. The model reproduces the correct trends for the sub 2 atm data, but under predicts reactivity, particularly at the lower temperatures of the study.

The effect of pressure on the ignition delay time can be observed in Fig. 36. This figure compares the H_2/O_2 data and the 10:90 H_2:CO for the three pressures investigated in this study. The effect of pressure on the ignition delay time is quite important, and is excellently reproduced by the current model. An increase in the pressure leads to a dramatic change in the activation energy, E_a, for the two mixtures considered. For the results obtained around 1.6 and 30 atm, the E_a increases from 57 kJ/mol at 1.65 atm to 378.5 kJ/mol at 30 atm for the H_2/O_2 mixture. The addition of carbon monoxide in the mixture leads to a decrease in the activation energy in comparison with the H_2/O_2 mixture, where E_a = 50 kJ/mol at 1.6 atm and 190 kJ/mol at 30 atm.

Another noticeable result from Figs. 33-36 is that H_2 is more reactive than CO and is driving the ignition of syngas mixtures, even if only 10% by volume of the fuel proportion is H_2, as shown in Fig. 33.

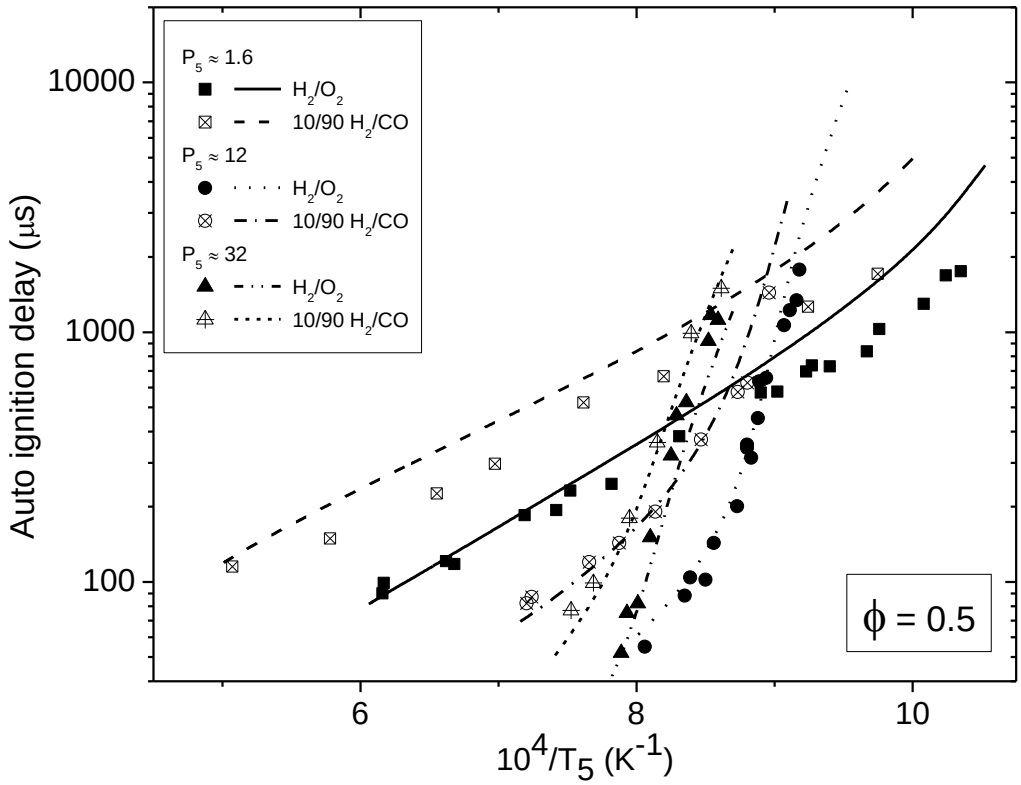

Fig. 36 Evolution of the ignition delay time with the inverse of the temperature for various pressures and for mixtures of H_2/O_2 and 10/90 H_2/CO (98% dilution in Ar, $\phi = 0.5$). Lines are model simulations.

CONCLUSION

Two high-precision experimental gas dynamic apparatuses were used to validate and produce new information on the combustion kinetics of hydrogen and syngas. The first device used was a constant-volume cylindrical bomb to measure laminar flame speeds. The current facility has two constant-volume cylindrical bombs: one capable of initial conditions only at room temperature and up to 15 atm and the other capable of initial temperatures and pressures up to 600 K and 30 atm, respectively. Laminar flame speed measurements were made at various conditions of hydrogen and syngas and compared to available literature information with generally good agreement, although variations as high as 34 cm/s are seen amongst the literature data at lean conditions. Additionally, a recently improved chemical kinetics model was shown to have overall very good agreement at the conditions presented herein. The second device used was a high-pressure shock tube. Several compositions of syngas were performed at a single equivalence ratio and 98% dilution at three pressures and compared to previously published hydrogen-oxygen data from our laboratory. The results showed that an increase in carbon monoxide in the fuel will increase the ignition delay time, but pressure appears to play a role on this result. Also, it was seen that the activation energy will decrease with increasing amounts of carbon monoxide. Both of these phenomena are accurately reproduced by the model.

The $H_2/O_2/NO_2$ system, highly diluted in Ar, was investigated thanks to shock-tube ignition delay time measurements with the purpose to understand the sensitizing effect of NO_2 addition on hydrogen oxidation. Experiments and computational simulations were performed at an equivalence ratio of 0.5, at pressures of approximately 1.5, 13 and 30 atm and at temperatures from 980 – 1750 K. At around 1.5 atm, the ignition delay time is not sensitive to additions of 100 or 400 ppm of NO_2. An addition of 1600 ppm will however increase the ignition delay time. At a pressure of 13.5 atm, the ignition delay time was significantly decreased by addition of 100 and 400 ppm below 1140 K. Above 1140 K, no effect on the ignition delay time was observed for a NO_2 addition of 400 ppm or less. A NO_2 addition of 1600 ppm will decrease the delay time compared to the neat hydrogen conditions below 1140 K. The delays are however longer than the delays obtained with 400 ppm of NO_2. Above 1140 K, the delay time is increased by this large addition of NO_2. At 30 atm, the delay time is decreased by NO_2 addition, the decrease being more important as the temperature is lowered. The delays obtained with 1600 ppm of NO_2 are slightly longer than the delays obtained with 400 ppm of NO_2. A sensitivity analysis was performed at 13.5 atm to help explain the interesting effects of the addition of various amounts of NO_2 on the ignition delay time. These experimental results were explained in terms of detailed kinetic reactions and chemical process using the sensitivity analysis.

Progress on Task 5 was made with respect to the tunable dye laser diagnostic to be used for measuring the concentration of NH in a shock tube using laser absorption in the ultraviolet. For Task 6, the baseline syngas mixtures were chosen, to be used for the future impurity studies.

COST STATUS

Provided below is the cost status through the fourth quarter.

Cooperative Agreement DE-FE0004679							Total Award: $501,712.0		PI: Eric Petersen			
Cost Plan /Status												
	Year 1 Start:		End:		Year 2 Start:		End:		Year 3 Start:		End:	
Baseline Reporting Quarter	Q1	Q2	Q3	Q4	Q5	Q6	Q7	Q8	Q9	Q10	Q11	Q12
Baseline Cost Plan	(From 424A, Sect D)				(From 424A, Sect E)							
(fromSF-424A)	265,206.00				145,535.00				90,971.00			
Federal Share	123,906.00	47,906.00	47,906.00	47,906.00								
Non-Federal Share	10,172.00	10,172.00	10,172.00	10,172.00								
Total Planned (Federal and Non-Federal)	134,078.00	58,078.00	58,078.00	58,078.00								
Cumulative Baseline Cost		192,156.00	250,234.00	308,312.00								
Actual Incurred Costs												
Federal Share	75,110.58	151,538.36	48,000.00	40,000.00								
Non-Federal Share	13,279.98	31,762.39	0.00	0.00								
Total Incurred Costs-Quarterly (Federal and Non-Federal)	88,390.56	183,300.75	48,000.00	40,000.00								
Cumulative Incurred Costs		271,691.31	319,691.00	359,691.00								
Variance												
Federal Share	-48,795.42	103,632.36	94.00	-7,906.00								
Non-Federal Share	3,107.98	21,590.39	-10,172.00	-10,172.00								
Total Variance-Quarterly (Federal and Non-Federal)	-45,687.44	125,222.75	-10,078.00	-18,078.00								
Cumulative Variance		79,535.31	69,275.31	51,379.00								

SCHEDULE/MILESTONE STATUS

Presented on the following page is the milestone chart through the fourth quarter.

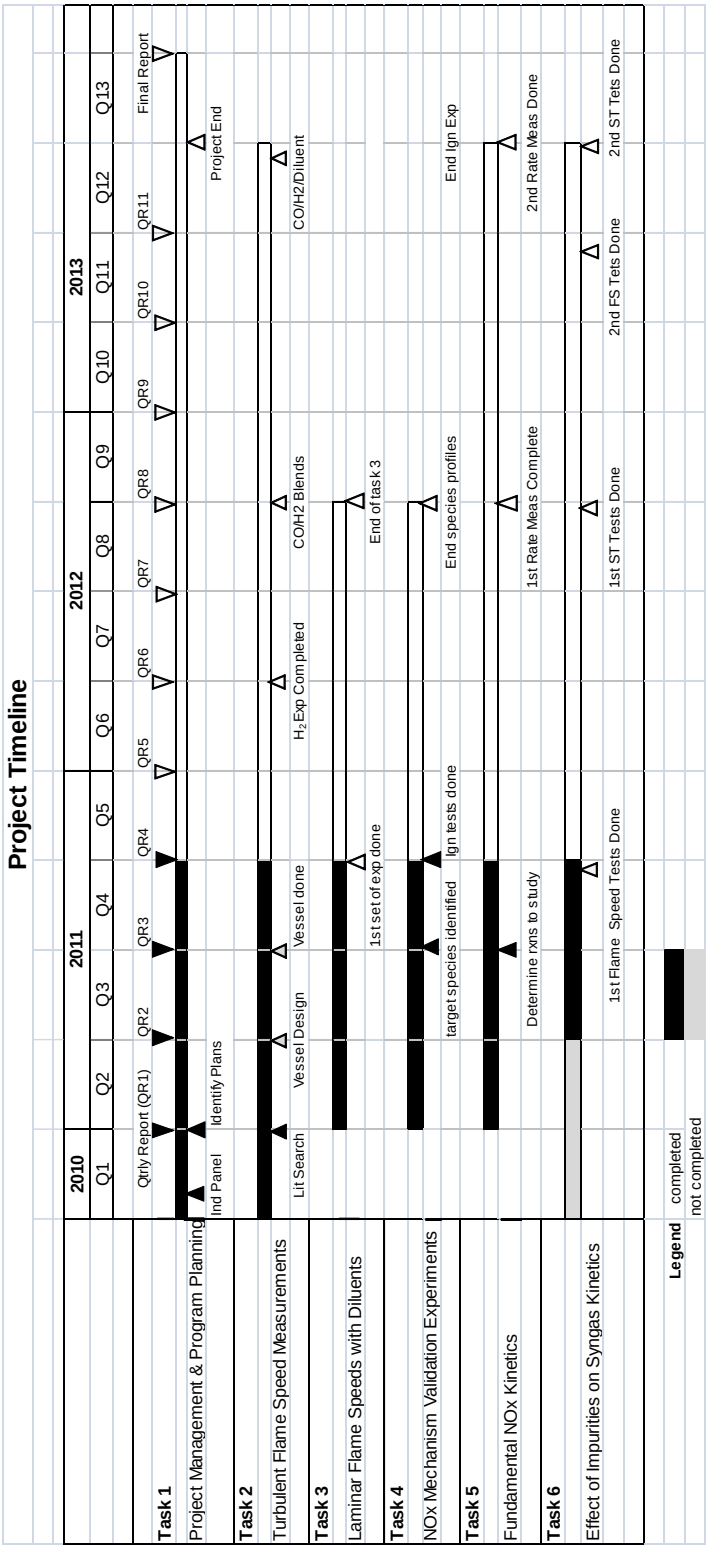

REFERENCES

Aung K. T., Hassan M. I., and Faeth G. M. (1997) "Flame Stretch Interactions of Laminar Premixed Hydrogen/Air Flames at Normal Temperature and Pressure," *Combustion and Flame*, Vol. 109, pp.1-24.

Bouvet N., Chauveau C., Gokalp I., and Halter F. (2011) "Experimental studies of the fundamental flame speeds of syngas (H_2/CO)/air mixtures," *Proceedings of the Combustion Institute*, Vol. 33, pp. 913-920.

Bozzelli, J. W. and Dean, A. M. (1995) *International Journal of Chemical Kinetics*, Vol. 27, pp. 1109-1109.

Bradley, D., Haq, M.Z., Hicks, R.A., Kitigawa, T., Lawes, M., Sheppard, C.G.W. and Woolley, R. (2003) "Turbulent Burning Velocity, Burned Gas Distribution, and Associated Flame Surface Definition," *Combustion and Flame*, Vol. 133, pp. 415-430.

Brown J.M., McLean I.C., Smith D. B., and Taylor S. C. (1996) "Markstein Lengths of CO/H_2/Air Flames, Using Expanding Spherical Flames," *Proceedings of the Combustion Institute*, Vol. 26, pp. 875-881.

Burke M. P., Qin X., Ju Y., and Dryer F. L. (2007) "Measurements of hydrogen syngas flame speeds at elevated pressures," 5th U.S. Combustion Meeting.

Burke M. P., Chen Z., Ju Y., and Dryer F. L. (2009) "Effect of cylindrical confinement on the determination of laminar flame speeds using outwardly propagating flames," *Combustion and Flame*, Vol. 156, pp. 771-779.

CHEMKIN-PRO 15101 (2010) Reaction Design: San Diego.

Dahoe A. E. (2005) "Laminar burning velocities of hydrogen-air mixtures from closed vessel gas explosions," *Journal of Loss Prevention in the Process Industries*, Vol. 18, pp. 152-166.

de Vries J., Lowry W., Serinyel Z., Curran H., and Petersen E. (2011) "Laminar flame speed measurements of dimethyl ether in air at pressures up to 10 atm," *Fuel*, 90(1), pp. 331-338.

Dong C., Zhou Q., Zhao Q., Zhang Y., Xu T., and Hui S. (2009) "Experimental study on the laminar flame speed of hydrogen/carbon monoxide/air mixtures," *Fuel*, Vol. 88, pp. 1858-1863.

Dowdy D. R., Smith D. B., Taylor S. C., and Williams A. (1990) "The use of expanding spherical flames to determine burning velocities and stretch effects in hydrogen/air mixtures," *Proceedings of the Combustion Institute*, Vol. 23, pp. 325-332.

Egolfopoulos F. N. and Law C. K. (1990) "An experimental and computational study of the burning rates of ultra-lean to moderately-rich $H_2/O_2/N_2$ laminar flames with pressure variations," *Proceedings of the Combustion Institute*, Vol. 23, pp. 333-340.

Haq, Md.Z. (1998) "Fundamental Studies of Premixed Combustion," PhD Thesis, Univ. of Leeds, Leeds, UK.

Hassan M. I., Aung K. T., and Faeth G. M. (1997) "Properties of laminar premixed CO/H_2/Air flames at various pressures," *Journal of Propulsion and Power*, Vol. 13, pp. 239-245.

Hu E., Huang Z., He J., Miao H. (2009) "Experimental and numerical study on laminar burning velocities and flame instabilities of hydrogen-air mixtures at elevated pressures and temperatures," *International Journal of Hydrogen Energy*, Vol. 34, pp. 8741-8755.

Hwang, W. and Eaton, J.K. (2004) "Creating Homogeneous Turbulence without a Mean Flow," *Experiments in Fluids*, Vol. 36, pp. 444-454.

Kéromnès, A., Metcalfe, W. K., Donohoe, N., Curran, H. J., and Pitz, W. J. (2011) "Detailed Chemical Kinetic Model for H_2 and H_2/CO (Syngas) Mixtures at Elevated Pressure," 7th US National Meeting of the Combustion Institute, March 21-23, Atlanta.

Kido, H., Tanoue, K., Nakahara, M., Kido, K. and Inoue, T. (1996) "Experimental Study on the Turbulent Combustion Mechanism of Non Stoichiometric Mixtures," *JSAE Review*, Vol. 17, pp. 361-367.

Konnov, A. A. and De Ruyck, J. (2001) *Combustion and Flame*, Vol. 125, pp. 1258-1264.

Krejci M., Vissotski A., Lowry W., Ravi S., and Petersen E. (2011) "Development of a High-Temperature and High-Pressure Vessel for Laminar Flame Speed Measurements," 7th U.S. National Technical Meeting.

Kwon, S.J. (1991) "Flame Surface Properties of Neutrally Stable Premixed Flames In Isotropic Turbulence," PhD Thesis, Univ. of Michigan, Ann Arbor, USA.

Kwon O. C. and Faeth G. M. (2001) "Flame/stretch interactions of premixed hydrogen-fueled flames: measurements and predictions," *Combustion and Flame*, Vol. 124, pp. 590-610.

Lamoureux N., Djebaili-Chaumeix N., and Paillard C. E. (2003) "Laminar flame velocity determination for H_2-air-He-CO_2 mixtures using the spherical bomb method," *Experimental Thermal and Fluid Science*, Vol. 27, pp.385-393.

Lipatnikov, A.N. and Chomiak, J. (2002) "Turbulent Flame Speed and Thickness: Phenomenology, Evaluation and Application in Multi-Dimensional Simulations," *Progress in Energy and Combustion Science,* Vol. 28, pp. 1-74.

Lowry W., de Vries J., Krejci M., Serinyel Z., Metcalfe W., Curran H., Petersen E., and Bourque G. (2011) "Laminar Flame Speed Measurements and Modeling of Pure Alkanes and Alkane Blends at Elevated Pressures," *Journal of Engineering for Gas Turbines and Power,* 133 (9).

Markstein G. H. (1964) *Non-Steady Flame Propagation*, Pergamon, New York.

McLean I. C., Smith D. B., and Taylor S.C. (1994) "The use of carbon monoxide/hydrogen burning velocities to examine the rate of the CO + OH reaction," *Proceedings of the Combustion Institute,* Vol. 25, pp. 749-757.

Moffat R. J. (1988) "Describing uncertainties in experimental results," *Experimental Thermal and Fluid Science,* Vol. 1, pp. 3-17.

Natarajan J., Nandula S., Lieuwen T., and Seitzman J. (2005) "Laminar flame speeds of synthetic gas fuel mixtures," ASME Paper GT2005-68917.

Ó Conaire, M., Curran, H. J., Simmie, J. M., Pitz, W. J., and Westbrook, C. K. (2004) "A Comprehensive Modeling Study of Hydrogen Oxidation," *International Journal of Chemical Kinetics*, Vol. 36, pp. 603–622.

Pareja J., Burbano H. J., and Ogami Y. (2010) "Measurements of the laminar burning velocity of hydrogen-air premixed flames," *International Journal of Hydrogen Energy*, Vol. 35, pp. 1812-1818.

Petersen E. L., Rickard M. J. A., Crofton M. W., Abbey E. D., Traum M. J., Kalitan D. M. (2005) "A facility for gas- and condensed-phase measurements behind shock waves," *Measurement Science and Technology*, Vol. 16, pp. 1716-1729.

Prathap C., Ray A., and Ravi M. R. (2008) "Investigation of nitrogen dilution effects on the laminar burning velocities and flame stability of syngas fuel at atmospheric condition," *Combustion and Flame,* Vol. 155, pp. 145-160.

Reynolds W. C. (1986) "The Element Potential Method for Chemical Equilibrium Analysis: Implementation in the Interactive Program STANJAN," Department of Mechanical Engineering, Stanford University.

Settles G. S. (2006) *Schlieren and Shadowgraph Techniques*, Springer, Heidelberg, Germany.

Sivaramakrishnan R., Brezinsky K., Dayma G., and Dagaut P. (2007) "High Pressure Effects on the Mutual Sensitization of the Oxidation of NO and CH_4-C_2H_6 Blends," *Physical Chemistry Chemical Physics*, Vol. 9, pp. 4230-4244.

Sun H., Yang S. I., Jomaas G., and Law C. K. (2007) “High-pressures laminar flame speeds and kinetic modeling of carbon monoxide/hydrogen combustion,” *Proceedings of the Combustion Institute*, Vol. 31, pp. 439-446.

Tse S.D., Zhu D. L., and Law C.K. (2000) “Morphology and burning rates of expanding spherical flames in H_2/O_2/inert mixtures up to 60 atmospheres,” *Proceedings of the Combustion Institute*, Vol. 28, pp.1793-1800.

Vagelopoulos C. M., Egolfopoulos F. N., and Law C. K. (1994) “Further considerations on the determination of laminar flame speeds with the counterflow twin-flame technique,” *Proceedings of the Combustion Institute*, Vol. 25, pp. 1341-1347.

Verhelst S., Woolley R., Lawes M., and Sierens R. (2005) “Laminar and unstable burning velocities and Markstein lengths of hydrogen-air mixtures at engine-like conditions,” *Proceedings of the Combustion Institute*, Vol. 30, pp. 209-216.

APPENDIX A – LAMINAR FLAME SPEED DATA

Table A1 Experimental results for atmospheric H_2-Air at initial temperatures of 298, 373, and 443 K.

ϕ	P_i (atm)	T_u (K)	σ	$S^0_{L,u}$ (cm/s)	L_m (cm)
0.5	1	295	5.041	64.7	-0.0086
0.6	1	297	5.562	94.3	-0.0057
0.7	1	298	6.012	124.4	-0.0020
0.8	1	298	6.391	169.9	0.0071
0.9	1	297	6.696	194.0	0.0083
1	1	295	6.894	218.0	0.0094
1.1	1	296	6.923	236.7	0.0088
1.2	1	298	6.855	254.9	0.0092
1.3	1	297	6.764	267.4	0.0089
1.4	1	295	6.669	275.0	0.0086
1.5	1	298	6.574	280.3	0.0089
1.6	1	296	6.480	282.8	0.0094
1.7	1	296	6.388	283.8	0.0097
1.8	1	295	6.298	282.9	0.0108
1.9	1	295	6.210	280.3	0.0118
2	1	298	6.124	278.9	0.0121
2.5	1	296	5.729	249.1	0.0145
3	1	296	5.385	217.4	0.0181
3.5	1	297	5.084	187.6	0.0216
4	1	296	4.821	158.7	0.0271
4.5	1	295	4.588	133.0	0.0366
5	1	295	4.381	110.1	0.0472
0.5	1	370	4.180	95.3	-0.0103
1.3	1	372	5.524	357.8	0.0069
1.7	1	370	5.237	383.5	0.0092
1.9	1	371	5.099	382.8	0.0116
3	1	372	4.456	310.3	0.0147
4	1	372	4.013	234.8	0.0205
0.5	1	444	3.639	141.2	-0.0062
0.8	1	444	4.498	314.9	0.0074
1.3	1	444	4.742	467.6	0.0074
1.7	1	444	4.512	499.6	0.0098
1.9	1	444	4.400	496.8	0.0095
2.5	1	443	4.094	458.3	0.0133
3	1	444	3.872	415.3	0.0148
3.5	1	443	3.677	367.7	0.0180
4	1	443	3.506	325.6	0.0191

Table A2 Experimental results for Hydrogen – 7:1 He:O_2 at 5 atm and initial temperatures of 298, 373, and 443 K and 10 atm at 298 K.

ϕ	P_i (atm)	T_u (K)	σ	$S^0_{L,u}$ (cm/s)	L_m (cm)
0.5	5	295	4.729	40.6	-0.0026
0.8	5	299	6.258	186.4	0.0045
1	5	298	6.960	245.3	0.0052
1.2	5	297	6.823	278.7	0.0027
1.5	5	297	6.482	300.5	0.0039
1.7	5	296	6.274	302.1	0.0047
1.8	5	295	6.176	286.4	0.0058
2.5	5	299	5.580	232.1	0.0084
3	5	297	5.232	182.1	0.0065
4	5	297	4.677	101.0	0.0176
0.5	5	371	3.961	81.5	-0.0013
1.1	5	371	5.692	386.9	0.0058
1.7	5	372	5.177	414.9	0.0041
1.8	5	372	5.099	392.3	0.0045
3	5	371	4.353	274.1	0.0004
4	5	372	3.913	155.3	0.0109
0.5	5	444	3.478	133.7	-0.0011
0.8	5	443	4.473	352.8	0.0038
1.1	5	443	4.906	497.6	0.0060
1.7	5	444	4.487	548.3	0.0039
1.8	5	443	4.422	519.2	0.0042
2.5	5	443	4.030	450.6	0.0047
3	5	444	3.800	398.6	0.0059
3.5	5	443	3.604	318.7	0.0072
4	5	443	3.433	257.3	0.0075
0.5	10	295	4.729	20.7	-0.0036
1.5	10	298	6.486	285.2	0.0021
1.7	10	295	6.277	273.6	0.0021
1.8	10	295	6.178	269.0	0.0030
1.9	10	295	6.083	271.4	0.0044
2.5	10	296	5.580	201.6	0.0040
3	10	298	5.233	161.5	0.0061
4	10	298	4.677	75.9	0.0264

Table A3 Experimental results for atmospheric 50:50 H_2:CO-Air at 298 K.

ϕ	P_i (atm)	T_u (K)	σ	$S^0_{L,u}$ (cm/s)	L_m (cm)
0.5	1	296	5.236	31.0	-0.0089
0.8	1	297	6.539	82.2	0.0025
1	1	296	6.911	114.1	0.0095
1.2	1	295	6.951	137.1	0.0089
1.5	1	296	6.697	166.7	0.0098
1.7	1	296	6.495	178.3	0.0072
1.8	1	296	6.396	182.1	0.0086
1.9	1	297	6.301	180.1	0.0079
2	1	295	6.209	188.7	0.0094
2.5	1	296	5.793	176.2	0.0112
3	1	295	5.440	154.7	0.0130
3.5	1	297	5.138	131.8	0.0177
4	1	295	4.876	105.9	0.0217

Table A4 Experimental results for 5-atm and 10-atm 50:50 H_2:CO – 7 He:O_2 at 298 K.

ϕ	P_i (atm)	T_u (K)	σ	$S^0_{L,u}$ (cm/s)	L_m (cm)
0.8	5	297	6.466	85.5	0.0052
1	5	296	7.046	130.5	0.0175
1.1	5	297	7.083	140.3	0.0084
1.7	5	295	6.392	180.4	0.0027
1.9	5	296	6.184	177.0	0.0040
2.5	5	296	5.657	144.5	0.0050
3	5	294	5.302	118.9	0.0077
4	5	297	4.747	60.2	0.0283
0.7	10	295	6.024	45.1	0.0037
1.5	10	298	6.625	169.0	0.0050
1.8	10	295	6.288	172.2	0.0045
2	10	298	6.088	163.7	0.0031
3	10	294	5.302	89.1	0.0038